O-antigen structure and surface hydrophobicity determines aggregate assembly type in *Pseudomonas aeruginosa*

Sheyda Azimi[1], Jacob Thomas[1], Sara E. Cleland[1], Jennifer E. Curtis[2], Joanna B. Goldberg[3] and Stephen P. Diggle[1]*

[1]*Center for Microbial Dynamics & Infection, School of Biological Sciences, Georgia Institute of Technology, Atlanta, U.S.A;* [2]*School of Physics, Georgia Institute of Technology, Atlanta, U.S.A.;* [3]*Division of Pulmonology, Allergy/Immunology, Cystic Fibrosis and Sleep, Department of Pediatrics, Emory University School of Medicine, Atlanta, U.S.A.*

*Correspondence: stephen.diggle@biosci.gatech.edu

Keywords: Lipopolysaccharide, O-antigen, *Pseudomonas aeruginosa*, cystic fibrosis, hydrophobicity, depletion aggregation

Abstract

Bacteria live in spatially organized aggregates during chronic infections, where they adapt to the host environment, evade immune responses and resist therapeutic interventions. Although it is known that environmental factors such as polymers influence bacterial aggregation, it is not clear how bacterial adaptation during chronic infection impacts the formation and spatial organization of aggregates in the presence of polymers. Here we show that in an *in vitro* model of cystic fibrosis (CF) containing the polymers eDNA and mucin, O-antigen is a major factor in determining the formation of two distinct aggregate assembly types of *Pseudomonas aeruginosa* due to alterations in cell surface hydrophobicity. Our findings suggest that during chronic infection, interplay between cell surface properties and polymers in the environment may influence the formation and structure of bacterial aggregates, which would shed new light on the fitness costs and benefits of O-antigen production in environments such as CF lungs.

Importance

During chronic infection, several factors contribute to the biogeography of microbial communities. Heterogeneous populations of *Pseudomonas aeruginosa* form aggregates in cystic fibrosis airways, however, the impact of this population heterogeneity on spatial organization and aggregate assembly is not well understood. In this study we found that changes in O-antigen structure determine the spatial organization of *P. aeruginosa* cells by altering the relative cell surface hydrophobicity. This finding

38 suggests a role for O-antigen in determining *P. aeruginosa* aggregate size and shape in cystic fibrosis
39 airways.
40
41 **Introduction**
42 During chronic infection, biofilm-forming cells are often more tolerant to antibiotics and the host immune
43 response than planktonic cells (1-3). Biofilms also allow individual cells the physical proximity to engage
44 in and benefit from social behaviors such as quorum sensing (QS) and the production of secreted common
45 goods (4-9). Biofilms formed during infection often take the form of cellular aggregates (8, 10-12). In the
46 fluids of wounds and airways of cystic fibrosis (CF) patients, the opportunistic pathogen *Pseudomonas*
47 *aeruginosa* frequently grows as freely suspended aggregates of ~10-10,000 cells (6, 8, 10, 11). The
48 mechanisms that govern the shape and size of bacterial aggregates during infection are not well defined.
49 In polymer rich environments, aggregates have been shown to form either by (i) an increase in entropic
50 force (depletion aggregation) (13, 14); or (ii) electrostatic interactions between bacterial cell surfaces and
51 polymers in the environment (bridging aggregation) (15-18).
52
53 *P. aeruginosa* populations become phenotypically and genetically diverse over time in the complex micro-
54 environments found in CF airways (19-22), and the importance of this heterogeneity on the formation and
55 organization of aggregates has not been assessed. To resolve this, we evaluated aggregate formation in
56 seven genetically diverse isolates sourced from heterogeneous populations of the *P. aeruginosa* strain
57 PAO1 previously evolved in biofilms for 50 days (23). We assessed how each isolate formed aggregates
58 in a polymer-enriched, spatially-structured CF growth medium (SCFM2: containing mucin and eDNA
59 polymers), which has previously been used as an *in vitro* CF model to study the biogeography and
60 physiology of *P. aeruginosa* (8, 24-26).
61
62 We found that the PAO1 ancestor and five isolates formed a stacked pattern (stacked aggregates) where
63 cells closely packed lengthwise, similar to those identified in previous polymer driven depletion-
64 aggregation studies (27). Two isolates formed distinct disorganized aggregates of varying sizes (clumped
65 aggregates), similar to aggregates previously observed in CF sputum samples (10, 28). Whole genome
66 sequencing showed that the two clumping isolates had alterations in the *ssg* gene (PA5001), which has
67 previously been shown to be involved in lipopolysaccharide (LPS) core and O-antigen biosynthesis (29-
68 32). In *P. aeruginosa*, LPS contains three major components: the lipid A layer of the outer membrane, a
69 core oligosaccharide and O-antigen components. O-antigens are further subdivided into a D-rhamnose
70 homopolymer found in most strains called the common polysaccharide antigen (CPA, formally A-band)

71 and a variable heteropolymer of 3 to 5 sugars called the O-specific antigen (OSA, formally B-band) that
72 confers serotype specificity (29, 32).
73
74 We hypothesized that changes in O-antigen glycoforms capping LPS would lead to different aggregate
75 assembly types by altering the physiochemical properties of the bacterial cell surface. This could result in
76 new interactions (e.g. between the bacteria or the bacteria and polymers) that compete with the entropic
77 force that otherwise leads to stacked aggregation in this polymer-rich environment. To elucidate the
78 contribution of LPS-capping glycoforms to aggregate assembly, we assessed the aggregate formation of
79 clean deletion mutants of OSA and CPA. We found that loss of OSA and changes in the capped LPS core
80 glycoforms led to increased hydrophobicity of the cell surface that overcame the entropic force imposed
81 by host polymers, resulting in disorganized, irreversible clumping. Most importantly, we demonstrate that
82 aggregate shape and structure is dependent on the interplay between the physical properties of the
83 environment and the biological mediation of bacterial cell surface properties governed by the LPS core
84 and O-antigen.
85
86 **Results**
87 **Distinct aggregate assembly types in genetically diverse *P. aeruginosa* isolates.** Genetic and
88 morphologically heterogeneous isolates of *P. aeruginosa* are commonly collected from expectorated CF
89 sputum samples (20, 21, 33, 34). Since it is known that several lineages of *P. aeruginosa* can stably coexist
90 in CF airways, we tested whether population heterogeneity impacted aggregate formation. We chose seven
91 distinct morphotypes isolated from a previous study where we evolved biofilms of PAO1 in a synthetic
92 polymer-free sputum media (SCFM) for 50 days (23, 35, 36) (Fig. S1A). We assessed aggregate formation
93 in a spatially structured iteration of SCFM termed SCFM2 which contains mucin and eDNA polymers
94 (24). We identified two distinct types of aggregate assembly, where PAO1 and five of the evolved isolates
95 (A2, B8, B13, C25 and D4) were assembled into stacked aggregates, where cells were closely aligned side
96 by side by entropic force, similar to previous reports (27) (Fig. 1A; Fig. S1B & C). In contrast, two of the
97 evolved isolates (A9, B9) formed clumped aggregates that appeared as disorganized small and large
98 groups of cells, similar to bridging aggregation (15) (Fig. 1A). We also investigated growth of A9 and B9
99 in SCFM (no addition of eDNA or mucin) and observed that both formed clumps even in a polymer free
100 environment, while the other isolates did not form any aggregates (Fig. S2A).
101
102 To identify genetic determinants of clumping assembly in the evolved isolates, we performed whole-
103 genome sequencing on each isolate using the Illumina Miseq platform. We used breseq (0.34.0) for variant

104 calling between the evolved isolates and the PAO1 ancestor (37). Whilst we found differential levels of
105 genetic variation in each isolate when compared to PAO1, we observed that A9 and B9 each contained a
106 1 bp deletion in the *ssg* gene (PA5001) (Dataset 1). To confirm that mutation of *ssg* results in a clumped
107 aggregate assembly, we complemented A9 and B9 with an intact *ssg* gene *in trans*. We found that in both
108 isolates, *ssg* complementation restored the stacked aggregate assembly seen in PAO1 (Fig. 1B; Fig. S2B)
109 suggesting that Ssg plays a role in aggregate assembly type.
110
111 A distinct feature of the stacked versus clumped aggregates was the average volume. We found that
112 stacked aggregate volumes were 2-4 times larger (median of ≈ 63 μm^3 and 89 μm^3 aggregate size for PAO1
113 and A2 respectively) and (median of ≈ 200 μm^3 in *ssg* complemented A9 and B9) compared to clumped
114 aggregates (median aggregate size of ≈ 23 and 30 μm^3 for A9 and B9 respectively) (Fig. 1B). To quantify
115 these observed differences in the distribution of aggregate biomass in cells with stacked and clumped
116 aggregate assembly types, we compared the distribution of biovolume (ratio of aggregate volume to
117 surface area) for each type of aggregate assembly in SCFM2. We found that regardless of the size, the
118 median biovolume in stacked aggregates was significantly higher than in clumped aggregates (Table S1).
119
120 **O-antigen structure and not other biofilm traits determines aggregate assembly type.** The proposed
121 function of Ssg is a glycosyltransferase, involved in LPS and exopolysaccharide biosynthesis (30, 38). *P.*
122 *aeruginosa* with mutations in *ssg* have previously been shown to display decreased motility, enhanced
123 phage resistance and a lack of O-antigen (30, 31, 39). We next determined whether the different aggregate
124 assemblies (due to the loss of *ssg* in our evolved PAO1 isolates) was because of differences in O-antigen
125 production. We constructed a clean *ssg* gene deletion in PAO1 (PAO1Δ*ssg*) and a range of isogenic LPS
126 synthesis or O-antigen assembly mutants. These were (i) mannose reductase (PAO1Δ*rmd* OSA^+, CPA^-);
127 (ii) epimerase (PAO1Δ*wbpM* OSA^-, CPA^+); (iii) OSA polymerase (PAO1Δ*wyz*, OSA^-, CPA^+); (iv)
128 common initiating glycosyltransferase (PAO1Δ*wbpL*, OSA^-, CPA^-) and (v) O-antigen ligase
129 (PAO1Δ*waaL,* OSA and CPA still made but not attached to LPS in the periplasm). In addition, we made
130 mutants in the high (PAO1Δ*wzz*1 OSA^+, CPA^+) and very high (PAO1Δ*wzz*2, OSA^+, CPA^+) OSA chain-
131 length regulators (40, 41) (Fig. S3). We then determined the aggregate assembly type of the O-antigen
132 mutants in SCFM2. We found that *ssg, wbpL* and *wbpM* mutants with no OSA, formed clumped
133 aggregates, but lack of CPA alone (PAO1Δ*rmd*) did not change the aggregate assembly type (Fig. 2A &
134 B).
135

136 Biofilm formation by *P. aeruginosa* is regulated by several well-described mechanisms such as
137 exopolysaccharide production, adhesins and quorum sensing (QS) (6, 9, 42, 43). To determine whether
138 any of these factors interfered with stacked aggregation in SCFM2, we examined the aggregate assembly
139 of defined mutants in exopolysaccharide production (PAO1Δ*pel/psl*), lectins (PAO1Δ*lecA* &
140 PAO1Δ*lecB*) and a mutant lacking a major QS regulator (PAO1Δ*lasR*). Although the role of QS and
141 biofilm formation remains controversial, we assessed this mutant because LasR regulates several
142 pathways that could impact on aggregation type (7, 44). We found that all these mutants displayed stacked
143 aggregate assembly like PAO1 (Fig. 3). This indicated that changes in aggregate assembly type was not
144 due to alterations in common phenotypes associated with biofilm formation, only the loss of OSA was
145 important.
146
147 **Loss of OSA leads to clumped aggregates, independent of polymer and cell density.** To determine
148 differences in stacked and clumped aggregate assembly in SCFM2, despite the presence of polymers, we
149 monitored aggregate assembly of PAO1 and PAO1Δ*wbpL* over time. We found that an increase in initial
150 cell density resulted in the rapid formation of stacked aggregates, while there were no changes in clumped
151 aggregate assembly (Movie S1 and S2).
152
153 When we monitored the aggregate formation of PAO1 and PAO1Δ*wbpL* over 6 h, we found that there
154 was a significant change in PAO1 aggregate biovolume after 180 min of cells growing in SCFM2 and
155 when the stacks were assembled (Fig. 4A) whereas, regardless of cell density, the biovolume of
156 PAO1Δ*wbpL* aggregates remained constant over time (Fig. 4B). We also found that reducing the
157 concentration of both polymers in SCFM2, led to the dissolution of stacked aggregates as expected, while
158 it did not affect the formation of PAO1Δ*wbpL* clumped aggregates (Fig. S4). These findings suggest that
159 loss of OSA prevents entropically-derived stacked aggregate assembly, and the associated mechanism is
160 independent of the polymer concentration and/or cell density. This is a well-studied manifestation of
161 aggregation of hydrophobic particles in colloidal environments (45, 46).
162
163 **Aggregate assembly of *P. aeruginosa* is not serotype specific but dependent on cell surface relative**
164 **hydrophobicity.** There are 20 serotypes of *P. aeruginosa* based on the glycosyl groups of OSA (38). As
165 our findings were limited to PAO1 (serotype O5), we examined aggregate formation of PA14 (serotype
166 O10), PAK (serotype O6) and STO1 (serotype O1) which all differ in the oligosaccharide units of OSA
167 (38). In all serotypes we observed a stacked assembly similar to PAO1, but in an STO1 strain lacking
168 OSA (Δ*wbpM*), we identified small clumped aggregates, with restoration of stacks when *wbpM* was

169 complemented *in trans* (Fig. 5A & B). This data confirms that aggregate assembly type is not serotype
170 specific.
171
172 Previously it has been shown that lack of OSA increases the hydrophobicity of the *P. aeruginosa* cell
173 surface (30). To determine whether hydrophobicity correlated with aggregate type, we assessed the
174 relative surface hydrophobicity of OSA+ and OSA- strains. We found a significant increase in surface
175 hydrophobicity in OSA mutants (Fig. 6A), which corresponded with a clumping aggregate phenotype
176 (Fig. 2). Loss of OSA is a common adaptive trait of *P. aeruginosa* in CF airways, possibly leading to
177 increase in cell surface hydrophobicity that could alter spatial organization of *P. aeruginosa* cells in CF
178 airways. We therefore evaluated the relative hydrophobicity of 11 *P. aeruginosa* isolates collected from
179 the expectorated sputa of 2 individuals with CF. We observed heterogeneity in cell surface relative
180 hydrophobicity of the CF isolates across the two patients (Fig. 6B).
181
182 **Discussion**
183 Despite a large body of work showing how *P. aeruginosa* adapts to the CF lung environment (19-21, 33,
184 47, 48), and population heterogeneity during chronic infection (20, 21, 23, 49, 50), little is known about
185 the impact of this intra-specific heterogeneity on the formation of *P. aeruginosa* aggregates. To test
186 whether genetic heterogeneity impacts aggregation, we investigated the aggregate formation of selected
187 evolved isolates from a previous 50-day biofilm evolution experiment of PAO1 (23) in SCFM2 (24). We
188 found that (i) there are two distinct types of aggregate assemblies formed by *P. aeruginosa* in SCFM2;
189 (ii) the OSA impacts aggregate assembly type and (iii) the loss of OSA and LPS core+1 increases the
190 hydrophobicity of the bacterial surface which prevents depletion aggregation.
191
192 Previously it was shown that aggregation of *P. aeruginosa* cells in a polymer rich environment can be due
193 to depletion forces, where reduction of the free energy by increased entropy of the whole system leads to
194 a stacked aggregation of bacterial cells (27). Change of the polymer electrostatic properties in the same
195 study, altered the aggregate assembly to bridging assembly, suggesting that aggregate assembly type is
196 driven by physical properties of the environment, and that the biological properties of the cells assumes
197 little or no role on aggregate assembly type (27). However, we observed two distinct types of aggregate
198 assembly by genetically diverse PAO1 isolates in SCFM2. Stacked aggregation is dependent on cell
199 density and polymer concentration, and that increase in entropy is the driving force behind these
200 assemblies. In contrast, clumping assembly is driven by changes in surface properties of *P. aeruginosa*
201 cells. This indicates that although aggregate formation is influenced by physical forces, O-antigen

202 structure strongly impacts upon the spatial organization enforced by physical properties of the
203 environment.
204
205 Other studies have suggested that during CF infection, polymers like mucin can disperse cells in
206 established biofilms (51), although our work suggests that polymers are more likely to influence the spatial
207 arrangement of the cells. The clumping aggregate assembly was not influenced by factors that have
208 previously been shown to be involved in biofilm and aggregate formation including lectins (42, 52), QS
209 (6, 9, 53) and EPS (54-57). While we found that stacked aggregates had a larger biovolume than clumped
210 aggregates, and this can be explained by depletion aggregation, other explanations also exist. First, stacked
211 aggregates might be more likely to support growth within the aggregate leading to larger aggregates.
212 Second, as clumped aggregates get larger, they may be more prone to disaggregation, leading to them
213 never achieving a larger size even if there were cellular division occurring in the aggregate.
214
215 It remains to be determined whether stacked aggregates are found during human CF infection, although a
216 recent study demonstrated that in CF airways, eDNA surrounds aggregates, suggesting that in CF lungs,
217 eDNA could increase entropic force and form aggregates via depletion aggregation (58). It is noteworthy
218 that stacked aggregates form in other species of bacteria such as in *Rhizobium leguminosarum* which was
219 dependent on LPS core and O-antigen (59). Further, honeycomb structures of *P. aeruginosa* (multi-layers
220 of stacks) were shown to form in the crops of *Drosophila melanogaster,* highlighting that stacked
221 aggregates are found in some types of infection (60).
222
223 By assessing the relative hydrophobicity of cells forming different aggregate types, we found that *P.*
224 *aeruginosa* cells that form clumped aggregates have higher relative hydrophobic surfaces. Regulating
225 aggregate assembly type by directly altering OSA expression levels in environments containing
226 differential levels of cells and polymers (such as CF sputum), may allow cells to better resist
227 environmental stressors such as the host immune response, antibiotics or phage. The loss of OSA has been
228 reported in *P. aeruginosa* strains isolated from CF sputum, suggesting that finding small, clumped
229 aggregates in CF sputum and CF airways (61), might be directly due to the loss of OSA. As our work was
230 performed *in vitro,* further studies are required to determine how OSA and surface hydrophobicity impacts
231 on aggregate formation in *P. aeruginosa* isolates growing in CF lungs.
232
233 Overall, our findings highlight that the surface properties of *P. aeruginosa* cells determines how they form
234 aggregates in environments with different physicochemical properties, providing potential benefits from

235 social interactions with highly-related cells. Our findings also highlight, that changes in cell surface
236 properties may influence how aggregates form in other species of bacteria and provides explanations as
237 to how different *P. aeruginosa* strains and species can stably co-exist in microbiomes.
238

239 **Materials & Methods**

240 **Bacterial strains and culture condition.** We selected 7 evolved isolates of PAO1 from 50 day evolved
241 populations in SCFM (23). We transformed all *P. aeruginosa* strains used in this study with pME6032:*gfp*
242 plasmid (62) using electroporation (63). Briefly, to prepare electrocompetent *P. aeruginosa* cells; we grew
243 the bacterial cells in LB broth overnight, we then washed the overnight cultures with 300 mM sucrose
244 solution at room temperature, and then resuspended the bacterial pellets in 1ml of 300 mM sucrose. We
245 then electroporated 50 µl of electrocompetent cells with 2 µl of purified plasmid and recovered the cells
246 by addition of 950 µl of LB broth and incubation at 37 ºC/ 200 rpm for 30 mins. We selected the
247 transformed cells by plating out the electroporated bacteria onto LB agar plates supplemented with 200
248 mg/ml of tetracycline. We obtained the clinical isolates from Emory CF@LANTA Research Center.
249 Patients in this study were aged between 21-29 at the time of collection of the sputum samples. This study
250 was approved by Institutional Review Board (IRB) at Georgia Institute of Technology and Emory
251 University Hospital. A list of all bacterial strains used in this study is available in Table S2.
252

253 **Determining diversity in colony morphologies.** To determine diversity in colony morphology in evolved
254 populations (23), we used a Congo Red based agar media (1% agar, 1×M63 salts (3g monobasic KHPO4,
255 7g K2PO4, 2g NH4.2SO4, pH adjusted to 7.4), 2.5 mM magnesium chloride, 0.4 mM calcium chloride,
256 0.1% casamino acids, 0.1% yeast extracts, 40 mg/l Congo red solution, 100 µM ferrous ammonium
257 sulphate and 0.4% glycerol) (64). We inoculated each evolved isolate in LB broth and incubated for 6 h
258 at 37ºC/200 *rpm,* then we spotted a 10 µl of the culture onto Congo Red agar plates. We incubated the
259 plated at 37ºC for 24 h and a further 4 days at room temperature.
260

261 **Genomic DNA extraction and whole genome sequencing.** We plated each of the selected evolved
262 isolates on LB agar plates, picked single colonies of each isolate and then inoculated in 5 ml of SCFM
263 (35) and incubated overnight at 37 ºC/ 200 rpm. We extracted the genomic DNA using the QIAGEN
264 Blood and Tissue DNAeasy kit. We prepared sequencing libraries using the NexteraXT protocol
265 (Illumina), and sequenced in 24-plex on the Illumina MiSeq platform to obtain an approximate calculated
266 level of coverage of 50× for each evolved isolate. For SNP calling, we used breseq analysis (consensus

267 mode) (37, 65, 66) and compared the genetic variation in each evolved isolate to the PAO1 ancestral
268 strain. The sequences are available at the NCBI SRA database (PRJNA702741).
269
270 **Image acquisition and analysis.** For imaging aggregates in SCFM2 (24), we inoculated each bacterial
271 isolate into TSB-broth supplemented with 200 µg/ml of tetracycline and incubated at 37 ºC/200 rpm
272 overnight. We inoculated 50 µl of the overnight culture into 5 ml of SCFM and incubated at 37 ºC/ 200
273 rpm for 5-6 h, until cultures reached mid-log phase (OD_{600}= 0.5). We then adjusted the OD_{600} to 0.05 in
274 400 µl of freshly made SCFM2 containing 0.6 mg/ml of DNA and 5 mg/ml of mucin (8, 24). We incubated
275 the cultures at 37 ºC for 16 h in chamber slides (Lab-Tek®) before image acquisition. We used a confocal
276 LSM880 microscope equipped with a 63× oil immersion lens for image acquisition and scanned the
277 aggregates using diode laser 488 nm, and collected fluorescent emission between 480-530 nm for image
278 acquisition. For imaging the cells grown in SCFM, we adjusted the OD_{600} of cells from mid-log phase
279 growth to 0.05 in 400 µl of freshly made SCFM. We incubated the cultures at 37 ºC for 16 h in chamber
280 slides before image acquisition. For image analysis, we used Imaris 9.0.1 image analysis software to
281 analyze the morphological properties of the aggregates and measured the surface area and volume of each
282 aggregate using a surface model algorithm. We used the same parameters for particle and voxel size. We
283 measured the aggregate volume and surface area in 10 images acquired for each strain in three independent
284 experiments (over 1000 aggregates were measured in total for each condition). For time course
285 experiments, we used the same image acquisition parameters, using the time series option and imaged as
286 Z stacks every 20 min for up to 10 h. To assess the role of bacterial cell density on aggregation, we adjusted
287 the OD_{600} to 0.1 in 400 µl of SCFM2 and imaged the cells every 20 min for 6 h. We prepared time series
288 videos using the 3D plugin in Fiji (67) and Adobe Lightroom.
289
290 **Gene deletion and complementation.** We used standard genetic techniques for the construction of *P.*
291 *aeruginosa* mutants. To delete *ssg*, *rmd*, *wbpL*, *wbpM*, *waaL*, *wzy*, *wzz1* and *wzz2,* we PCR amplified 600
292 bp DNA sequences flanking the open reading frame of each gene using Q5 DNA polymerase (New
293 England Biolabs). We then cloned these sequences into EcoRI-XbaI digested pEXG2 by Gibson assembly
294 using NEBuilder HiFi Assembly master mix (New England Biolabs) and transformed into *E.coli* S17 λpir.
295 We verified cloned inserts by colony PCR and Sanger sequencing (Eurofins Genomics). We introduced
296 the deletion constructs into PAO1 by electroporation and selected strains carrying single crossover
297 insertions of the deletion constructs on LB agar plates supplemented with 100 µg/ml gentamycin. We
298 cultured gentamycin resistant colonies in LB without antibiotic and plated on LB agar plates with 0.25%
299 NaCl and 5% sucrose. We then selected sucrose resistant colonies and screened them for gentamycin

300 sensitivity to ensure loss of the pEXG2 construct and assessed them for the desired gene deletion by colony
301 PCR and Sanger sequencing of the PCR product. For *ssg* complementation we PCR amplified the *ssg*
302 coding sequence and 100 bp upstream sequence (including the *ssg* native promoter) using Q5 DNA
303 polymerase (New England Biolabs). We cloned this 1057 bp product into KpnI-BamHI digested pUC18T-
304 miniTn7-Gent by Gibson assembly using NEBuilder HiFi Assembly master mix (New England Biolabs)
305 and transformed into *E.coli* S17 λpir. We verified the cloned insert by colony PCR and Sanger sequencing
306 (Eurofins Genomics). We co-transformed the complementation construct with the Tn7 helper plasmid
307 pTNS3 into PAO1Δ*ssg* and evolved isolates by electroporation and selected on LB agar plates
308 supplemented with 100 µg/ml gentamycin. We verified the strains for *ssg*+ complementation by colony
309 PCR and for loss of pUC18-miniTn7-Gent vector and pTNS3 by screening for carbenicillin sensitivity.
310
311 **LPS extraction.** We isolated bacterial lipopolysaccharide by the hot phenol extraction method (68).
312 Briefly, we pelleted 5 ml overnight cultures of PAO1 and PAO1-derived strains in LB broth by
313 centrifugation for 10 min at 4200×g. We resuspended the pellets in 200 µl 1X SDS buffer (2% β-
314 mercaptoethanol (BME), 2% SDS, 10% glycerol, 50 mM Tris-HCl, pH 6.8) and incubated at 99°C for 15
315 min. Then we added 5 µl of 20 mg/ml proteinase K (Sigma) to each tube and incubated cell lysates at
316 59°C for 3 hours. Then we added 200 µl of ice-cold Tris-saturated phenol to each sample, vortexed for 10
317 min, then added 1 ml diethyl-ether and vortexed for a further 10 seconds. We centrifuged the samples for
318 10 min at 16000×g and extracted the bottom layer. We performed a second extraction with phenol and
319 diethyl-ether as above. We mixed an equal volume of the extracted LPS samples with an equal volume of
320 2× SDS buffer and electrophoresed 10 µl of each sample on Novex 4-20% plyacrylamide gradient gels
321 (ThermoFisher) in Tris-Glycine-SDS buffer. Following electrophoresis, we visualized LPS with a ProQ
322 Emerald Lipopolysaccharide staining kit (ThermoFisher).
323
324 **Assessing cell surface hydrophobicity.** To assess the levels of cell surface hydrophobicity, we used
325 hydrophobic interaction chromatography (29). Briefly, we grew bacterial cells for 6-8 h at 37 ºC/ 200 *rpm,*
326 to reach mid-log phase. We harvested the cells and washed the cells 3× with ice cold 3M NaCl pH=7 and
327 resuspended in 3M NaCl. We used octyl-Sepharose CL-4C beads (SIGMA) to assess the interaction of
328 hydrophobic cells to these beads compared to control Sepharose CL-4C beads (SIGMA). We prepared
329 bead columns by a 3× wash of the beads with Mili-Q water, and then 3× washes with 3M NaCl (pH=7)
330 (at 4ºC). We then prepared 1 ml columns of both beads by using 3 ml diameter filter paper. We added 100
331 µl of bacterial suspension and incubated at room temperature for 15 min. We measured the OD_{450} of flow

through from each column. We calculated the relative hydrophobicity based on the ratio of OD_{450} octyl-Sepharose CL-C4 column flow through and control column.

Statistical analysis. For statistical analysis of the aggregate volume and biovolume distribution, we used GraphPad Prism 8.0.

Figure legends

Fig. 1. The two types of aggregate assembly formed by *P. aeruginosa* isolates in SCFM2 is due to *ssg* gene mutation. (A) In PAO1 and evolved isolates, aggregates assembled into either organized stacked structures (labeled as S) or disorganized clumps (labeled as C). (B) Stacked aggregates of PAO1 and A2 were significantly larger than aggregates formed by A9 and B9, and complementation with an intact *ssg* gene significantly increased the aggregate volume (Kruskal-Wallis, Dunn's multiple comparison test, $p<0.0001$; error bars are median with interquartile range of aggregate volume, each data point is representative of an aggregate).

Fig. 2. Loss of OSA leads to clumped aggregate assembly. (A) Loss of CPA (Δ*rmd*) did not alter the type of aggregate assembly, and loss of OSA (Δ*wbpM*) lead to dispersed small aggregates. The loss of both CPA and OSA(Δ*wbpL*) changed aggregate assembly type similar to the *ssg* mutant. (B) There was a significant reduction in aggregate volume in *ssg, wbpL* and *wbpM* mutants, however only the loss of *ssg* and *wbpL* displayed large, clumped aggregates (Kruskal-Wallis, Dunn's multiple comparison test, $p<0.0001$; error bars are median with interquartile range of aggregate volume, each point is representative of an aggregate).

Fig. 3. The aggregate assembly type is independent of exoploysaccharide production, lectins and quorum sensing. (A) Loss of lectins (Δ*lecA* and Δ*lecB*), quorum sensing (Δ*lasR*) and exopolysaccharide components (Δ*pel/psl*) did not change the aggregate assembly type and aggregates were assembled in stacked form similar to those seen in PAO1. (B) Stacked aggregates formed by cells lacking lectins (Δ*lecA* and Δ*lecB*), quorum sensing (Δ*lasR*) and exopolysaccharide components (Δ*pel/psl*) were the same size as PAO1 aggregates (Kruskal-Wallis, Dunn's multiple comparison test, $p=0.1$, $p=0.6$, $p>0.999$ and $p>0.999$ when aggregate volumes of Δ*lecA,* Δ*lecB,* Δ*lasR* and Δ*pel/psl* were compared to PAO1; error bars are median with interquartile range of aggregate volume).

365 **Fig. 4. Clumped aggregate assembly is not dependent on cell density.** (A) The aggregate biovolume
366 of PAO1 significantly increased after 180 min of growth (median biovolume = 0.34-0.75 over time). (B)
367 In PAO1Δ*wbpL* (lacking OSA), biovolume remained the same over time (median biovolume = 0.33-0.27
368 over time).
369
370 **Fig. 5. Clumped Aggregate assembly of *P. aeruginosa* is not serotype specific.** (A) *P. aeruginosa* PA14
371 and PAK and STO1 formed stacked aggregates in SCFM2 and OSA$^-$ mutant STO1 (STO1Δ*wbpM*) lead
372 to clumped assembly of aggregates. (B) Loss of OSA altered aggregate assembly from stacked to clumped
373 in STO1 and significantly decreased aggregate volume (Kruskal-Wallis, Dunn's multiple comparison test,
374 p = 0.0048; error bars are median with interquartile range of aggregate volume, each data point is
375 representative of an aggregate).
376
377 **Fig. 6. Cell surface hydrophobicity determines the aggregate assembly type.** (A) The relative cell
378 surface hydrophobicity was dependent on OSA, and mutation in *ssg, wbpL* and *wbpM* lead to an increase
379 in relative hydrophobicity in PAO1 and STO1 (Green bars).
380
381 **Supplemental figure legends**
382
383 **Fig. S1. Aggregate assembly of PAO1 evolved isolates in SCFM2.** (A) Evolved isolates of PAO1
384 displayed differential colony morphologies on Congo red agar plates. (B) Evolved isolates B8, B13, C25
385 and D4 displayed stacked aggregate assembly (labeled as S). (C) There were no significant differences in
386 the volume of stacked aggregates in these isolates compared to PAO1 (p <0.0001, Kruskal-Wallis, Dunn's
387 multiple comparison test, error bars are median with interquartile range of aggregate volume).
388
389 **Fig. S2. Mutation in PA5001 (*ssg*) in PAO1 switches the stacked aggregate assembly to clumped**
390 **assembly.** (A) PAO1 and A2 cells formed a dispersed layer of cells on cover slips when grown in SCFM
391 (without any polymer), while A9 and B9 formed small clumps in SCFM. (B) Complementing A9 and B9
392 isolates with *ssg* restored the aggregate assembly to stacked (Kruskal-Wallis, Dunn's multiple comparison
393 test, p<0.0001, error bars are median with interquartile range of aggregate volume).
394
395 **Fig. S3. Loss of *ssg* function changes the LPS OSA profile in *P. aeruginosa.*** (A) Evolved isolates of
396 PAO1 with 1 bp deletion in *ssg* had the same OSA profile as PAO1Δ*ssg*, and complementation of *ssg* in

397 *trans* restored the OSA pattern. (B) Loss of *ssg* resulted in the loss of OSA and a change in capped core
398 pattern.
399
400 **Fig. S4. Stacked aggregate assembly is dependent on the concentration of both eDNA and mucin.**
401 (A) Stacked aggregate formation was disrupted by diluting polymers in SCFM2. (B) Clumped aggregate
402 assembly was independent of the polymer concentration in the environment.
403
404 **Movie S1. Increased cell density reduced the time of stacked aggregation.** To determine whether
405 stacked aggregate assembly was dependent on cell density, we monitored the growth of PAO1 over time
406 (initial density adjusted OD_{600} to 0.1 in 400 µl of SCFM2). Stacked aggregates were assembled after 180
407 min of growth.
408
409 **Movie S2. Increased cell density does not impact the timing of formation of clumped aggregation.**
410 We monitored the growth of PAO1Δ*wbpL* (initial density adjusted OD_{600} to 0.1 in 400 µl of SCFM2).
411 There was no change in aggregate assembly over time.
412
413 **Dataset 1. List of SNPs in 7 evolved isolates of PAO1.**
414
415 **Table S1. Stacked aggregates have higher biovolume than clumped aggregates.** To determine the
416 differences in biomass of each aggregate type, we calculated the total biovolume ($\mu m^3/\mu m^2$) of all
417 aggregates in each acquired image, using Imaris. There was a significant difference between distribution
418 of biovolume of stacked and clumped (green) aggregates (Kruskal-Wallis, Dunn's multiple comparison
419 test, $p<0.0001$; error bars are median with interquartile range of aggregate biovolume).
420
421 **Table S2. List of the strains used in this study.**
422
423 **Acknowledgments.** For funding, we thank the Georgia Institute of Technology; The Cystic Fibrosis
424 Foundation for grants (DIGGLE18I0; DIGGLE20G0) to SPD and a Fellowship to SA (AZIMI18F0);
425 CF@LANTA for a Fellowship to SA (3206AXB); The National Institute for Health (R01AI153116) to
426 SPD; the National Science Foundation (1806606) to JEC. We thank Marvin Whiteley for useful discussion
427 and use of his Confocal Ziess LSM880 and Imaris image analysis platform. Access to the CF Biospecimen
428 Registry (CFBR) at Emory Children's Center for Cystic Fibrosis and Airways Disease Research was

429 provided through Children's Healthcare of Atlanta and the Emory University Pediatric CF Discovery
430 Core. We thank Arlene Stecenko and Katy Clemmer for assistance acquiring bacterial isolates.
431
432 **Conflict of interest statement.** The authors declare no conflict of interest with any of the work presented
433 in this manuscript.
434
435 **References**
436
437 1. Kragh KN, Alhede M, Jensen PO, Moser C, Scheike T, Jacobsen CS, Seier Poulsen S, Eickhardt-
438 Sorensen SR, Trostrup H, Christoffersen L, Hougen HP, Rickelt LF, Kuhl M, Hoiby N, Bjarnsholt T.
439 2014. Polymorphonuclear leukocytes restrict growth of *Pseudomonas aeruginosa* in the lungs of cystic
440 fibrosis patients. Infect Immun 82:4477-86.
441 2. Hall CW, Mah TF. 2017. Molecular mechanisms of biofilm-based antibiotic resistance and
442 tolerance in pathogenic bacteria. FEMS Microbiol Rev 41:276-301.
443 3. Pang Z, Raudonis R, Glick BR, Lin TJ, Cheng Z. 2019. Antibiotic resistance in *Pseudomonas*
444 *aeruginosa*: mechanisms and alternative therapeutic strategies. Biotechnol Adv 37:177-192.
445 4. West SA, Griffin AS, Gardner A, Diggle SP. 2006. Social evolution theory for microorganisms.
446 Nat Rev Microbiol 4:597-607.
447 5. Xavier JB, Foster KR. 2007. Cooperation and conflict in microbial biofilms. Proc Natl Acad Sci
448 U S A 104:876-81.
449 6. Whiteley M, Diggle SP, Greenberg EP. 2017. Progress in and promise of bacterial quorum
450 sensing research. Nature 551:313-320.
451 7. Popat R, Crusz SA, Messina M, Williams P, West SA, Diggle SP. 2012. Quorum-sensing and
452 cheating in bacterial biofilms. Proc Biol Sci 279:4765-71.
453 8. Darch SE, Simoska O, Fitzpatrick M, Barraza JP, Stevenson KJ, Bonnecaze RT, Shear JB,
454 Whiteley M. 2018. Spatial determinants of quorum signaling in a *Pseudomonas aeruginosa* infection
455 model. Proc Natl Acad Sci U S A 115:4779-4784.
456 9. Azimi S, Klementiev AD, Whiteley M, Diggle SP. 2020. Bacterial Quorum Sensing During
457 Infection. Annu Rev Microbiol 74:201-219.
458 10. Bjarnsholt T, Alhede M, Alhede M, Eickhardt-Sorensen SR, Moser C, Kuhl M, Jensen PO,
459 Hoiby N. 2013. The *in vivo* biofilm. Trends Microbiol 21:466-74.
460 11. Roberts AE, Kragh KN, Bjarnsholt T, Diggle SP. 2015. The Limitations of *In Vitro*
461 Experimentation in Understanding Biofilms and Chronic Infection. J Mol Biol 427:3646-61.
462 12. Kragh KN, Hutchison JB, Melaugh G, Rodesney C, Roberts AE, Irie Y, Jensen PO, Diggle SP,
463 Allen RJ, Gordon V, Bjarnsholt T. 2016. Role of Multicellular Aggregates in Biofilm Formation. mBio
464 7:e00237.
465 13. Liu HH, Yang YR, Shen XC, Zhang ZL, Shen P, Xie ZX. 2008. Role of DNA in bacterial
466 aggregation. Curr Microbiol 57:139-44.
467 14. Dorken G, Ferguson GP, French CE, Poon WC. 2012. Aggregation by depletion attraction in
468 cultures of bacteria producing exopolysaccharide. J R Soc Interface 9:3490-502.
469 15. Harris RH, Mitchell R. 1973. The role of polymers in microbial aggregation. Annu Rev
470 Microbiol 27:27-50.
471 16. Strand SP, Nordengen T, Ostgaard K. 2002. Efficiency of chitosans applied for flocculation of
472 different bacteria. Water Res 36:4745-52.
473 17. Schweizer JBHaKS. 2005. Contact Aggregation, Bridging, and Steric Stabilization in Dense
474 Polymer−Particle Mixtures. Macromolecules 38:8858-8869.

475 18. Das T, Sharma PK, Busscher HJ, van der Mei HC, Krom BP. 2010. Role of extracellular DNA in
476 initial bacterial adhesion and surface aggregation. Appl Environ Microbiol 76:3405-8.
477 19. Marvig RL, Sommer LM, Molin S, Johansen HK. 2015. Convergent evolution and adaptation of
478 *Pseudomonas aeruginosa* within patients with cystic fibrosis. Nat Genet 47:57-64.
479 20. Darch SE, McNally A, Harrison F, Corander J, Barr HL, Paszkiewicz K, Holden S, Fogarty A,
480 Crusz SA, Diggle SP. 2015. Recombination is a key driver of genomic and phenotypic diversity in a
481 *Pseudomonas aeruginosa* population during cystic fibrosis infection. Sci Rep 5:7649.
482 21. Williams D, Evans B, Haldenby S, Walshaw MJ, Brockhurst MA, Winstanley C, Paterson S.
483 2015. Divergent, coexisting *Pseudomonas aeruginosa* lineages in chronic cystic fibrosis lung infections.
484 Am J Respir Crit Care Med 191:775-85.
485 22. Rossi E, La Rosa R, Bartell JA, Marvig RL, Haagensen JAJ, Sommer LM, Molin S, Johansen
486 HK. 2020. *Pseudomonas aeruginosa* adaptation and evolution in patients with cystic fibrosis. Nat Rev
487 Microbiol doi:10.1038/s41579-020-00477-5.
488 23. Azimi S, Roberts AEL, Peng S, Weitz JS, McNally A, Brown SP, Diggle SP. 2020. Allelic
489 polymorphism shapes community function in evolving *Pseudomonas aeruginosa* populations. ISME J
490 doi:10.1038/s41396-020-0652-0.
491 24. Turner KH, Wessel AK, Palmer GC, Murray JL, Whiteley M. 2015. Essential genome of
492 *Pseudomonas aeruginosa* in cystic fibrosis sputum. Proc Natl Acad Sci U S A 112:4110-5.
493 25. Cornforth DM, Dees JL, Ibberson CB, Huse HK, Mathiesen IH, Kirketerp-Moller K, Wolcott
494 RD, Rumbaugh KP, Bjarnsholt T, Whiteley M. 2018. *Pseudomonas aeruginosa* transcriptome during
495 human infection. Proceedings of the National Academy of Sciences of the United States of America
496 115:E5125-E5134.
497 26. Cornforth DM, Diggle FL, Melvin JA, Bomberger JM, Whiteley M. 2020. Quantitative
498 Framework for Model Evaluation in Microbiology Research Using *Pseudomonas aeruginosa* and Cystic
499 Fibrosis Infection as a Test Case. mBio 11.
500 27. Secor PR, Michaels LA, Ratjen A, Jennings LK, Singh PK. 2018. Entropically driven
501 aggregation of bacteria by host polymers promotes antibiotic tolerance in *Pseudomonas aeruginosa*.
502 Proc Natl Acad Sci U S A 115:10780-10785.
503 28. DePas WH, Starwalt-Lee R, Van Sambeek L, Ravindra Kumar S, Gradinaru V, Newman DK.
504 2016. Exposing the Three-Dimensional Biogeography and Metabolic States of Pathogens in Cystic
505 Fibrosis Sputum via Hydrogel Embedding, Clearing, and rRNA Labeling. mBio 7.
506 29. Makin SA, Beveridge TJ. 1996. The influence of A-band and B-band lipopolysaccharide on the
507 surface characteristics and adhesin of *Pseudomonas aeruginosa* to surfaces. Microbiology 142:299-307.
508 30. Veeranagouda Y, Lee K, Cho AR, Cho K, Anderson EM, Lam JS. 2011. Ssg, a putative
509 glycosyltransferase, functions in lipo- and exopolysaccharide biosynthesis and cell surface-related
510 properties in *Pseudomonas alkylphenolia*. FEMS Microbiol Lett 315:38-45.
511 31. Pan X, Cui X, Zhang F, He Y, Li L, Yang H. 2016. Genetic Evidence for O-Specific Antigen as
512 Receptor of *Pseudomonas aeruginosa* Phage K8 and Its Genomic Analysis. Front Microbiol 7:252.
513 32. Rocchetta HL, Burrows LL, Lam JS. 1999. Genetics of O-antigen biosynthesis in *Pseudomonas*
514 *aeruginosa*. Microbiol Mol Biol Rev 63:523-53.
515 33. Marvig RL, Dolce D, Sommer LM, Petersen B, Ciofu O, Campana S, Molin S, Taccetti G,
516 Johansen HK. 2015. Within-host microevolution of *Pseudomonas aeruginosa* in Italian cystic fibrosis
517 patients. BMC Microbiol 15:218.
518 34. Jorth P, Staudinger BJ, Wu X, Hisert KB, Hayden H, Garudathri J, Harding CL, Radey MC,
519 Rezayat A, Bautista G, Berrington WR, Goddard AF, Zheng C, Angermeyer A, Brittnacher MJ,
520 Kitzman J, Shendure J, Fligner CL, Mittler J, Aitken ML, Manoil C, Bruce JE, Yahr TL, Singh PK.
521 2015. Regional Isolation Drives Bacterial Diversification within Cystic Fibrosis Lungs. Cell Host
522 Microbe 18:307-19.

523 35. Palmer KL, Mashburn LM, Singh PK, Whiteley M. 2005. Cystic fibrosis sputum supports
524 growth and cues key aspects of *Pseudomonas aeruginosa* physiology. J Bacteriol 187:5267-77.
525 36. Palmer KL, Aye LM, Whiteley M. 2007. Nutritional cues control *Pseudomonas aeruginosa*
526 multicellular behavior in cystic fibrosis sputum. J Bacteriol 189:8079-87.
527 37. Barrick JE, Colburn G, Deatherage DE, Traverse CC, Strand MD, Borges JJ, Knoester DB, Reba
528 A, Meyer AG. 2014. Identifying structural variation in haploid microbial genomes from short-read
529 resequencing data using breseq. BMC Genomics 15:1039.
530 38. Huszczynski SM, Lam JS, Khursigara CM. 2019. The Role of *Pseudomonas aeruginosa*
531 Lipopolysaccharide in Bacterial Pathogenesis and Physiology. Pathogens 9.
532 39. Li Y, Xia H, Bai F, Song X, Zhuang L, Xu H, Zhang X, Zhang X, Qiao M. 2020. PA5001 gene
533 involves in swimming motility and biofilm formation in *Pseudomonas aeruginosa*. Microb Pathog
534 144:103982.
535 40. Kintz E, Goldberg JB. 2008. Regulation of lipopolysaccharide O antigen expression in
536 *Pseudomonas aeruginosa*. Future Microbiol 3:191-203.
537 41. Cross AR, Goldberg JB. 2019. Remodeling of O Antigen in Mucoid *Pseudomonas aeruginosa*
538 via Transcriptional Repression of *wzz2*. mBio 10.
539 42. Diggle SP, Stacey RE, Dodd C, Camara M, Williams P, Winzer K. 2006. The galactophilic
540 lectin, LecA, contributes to biofilm development in *Pseudomonas aeruginosa*. Environ Microbiol
541 8:1095-104.
542 43. Colvin KM, Gordon VD, Murakami K, Borlee BR, Wozniak DJ, Wong GC, Parsek MR. 2011.
543 The pel polysaccharide can serve a structural and protective role in the biofilm matrix of *Pseudomonas*
544 *aeruginosa*. PLoS Pathog 7:e1001264.
545 44. Rumbaugh KP, Griswold JA, Hamood AN. 2000. The role of quorum sensing in the in vivo
546 virulence of *Pseudomonas aeruginosa*. Microbes Infect 2:1721-31.
547 45. Lopez-Leon T, Ortega-Vinuesa JL, Bastos-Gonzalez D. 2012. Ion-specific aggregation of
548 hydrophobic particles. Chemphyschem 13:2382-91.
549 46. Sanchez-Iglesias A, Grzelczak M, Altantzis T, Goris B, Perez-Juste J, Bals S, Van Tendeloo G,
550 Donaldson SH, Jr., Chmelka BF, Israelachvili JN, Liz-Marzan LM. 2012. Hydrophobic interactions
551 modulate self-assembly of nanoparticles. ACS Nano 6:11059-65.
552 47. Marvig RL, Damkiaer S, Khademi SM, Markussen TM, Molin S, Jelsbak L. 2014. Within-host
553 evolution of *Pseudomonas aeruginosa* reveals adaptation toward iron acquisition from hemoglobin.
554 mBio 5:e00966-14.
555 48. Smith EE, Buckley DG, Wu Z, Saenphimmachak C, Hoffman LR, D'Argenio DA, Miller SI,
556 Ramsey BW, Speert DP, Moskowitz SM, Burns JL, Kaul R, Olson MV. 2006. Genetic adaptation by
557 *Pseudomonas aeruginosa* to the airways of cystic fibrosis patients. Proc Natl Acad Sci U S A 103:8487-
558 92.
559 49. Workentine ML, Sibley CD, Glezerson B, Purighalla S, Norgaard-Gron JC, Parkins MD, Rabin
560 HR, Surette MG. 2013. Phenotypic heterogeneity of *Pseudomonas aeruginosa* populations in a cystic
561 fibrosis patient. PLoS One 8:e60225.
562 50. Mei M, Thomas J, Diggle SP. 2021. Heterogenous Susceptibility to R-Pyocins in Populations of
563 *Pseudomonas aeruginosa* Sourced from Cystic Fibrosis Lungs. mBio 12.
564 51. Co JY, Carcamo-Oyarce G, Billings N, Wheeler KM, Grindy SC, Holten-Andersen N, Ribbeck
565 K. 2018. Mucins trigger dispersal of *Pseudomonas aeruginosa* biofilms. NPJ Biofilms Microbiomes
566 4:23.
567 52. Passos da Silva D, Matwichuk ML, Townsend DO, Reichhardt C, Lamba D, Wozniak DJ, Parsek
568 MR. 2019. The *Pseudomonas aeruginosa* lectin LecB binds to the exopolysaccharide Psl and stabilizes
569 the biofilm matrix. Nat Commun 10:2183.
570 53. Davies DG, Parsek MR, Pearson JP, Iglewski BH, Costerton JW, Greenberg EP. 1998. The
571 involvement of cell-to-cell signals in the development of a bacterial biofilm. Science 280:295-8.

572 54. Ma L, Wang S, Wang D, Parsek MR, Wozniak DJ. 2012. The roles of biofilm matrix
573 polysaccharide Psl in mucoid Pseudomonas aeruginosa biofilms. FEMS Immunol Med Microbiol
574 65:377-80.
575 55. Jennings LK, Storek KM, Ledvina HE, Coulon C, Marmont LS, Sadovskaya I, Secor PR, Tseng
576 BS, Scian M, Filloux A, Wozniak DJ, Howell PL, Parsek MR. 2015. Pel is a cationic exopolysaccharide
577 that cross-links extracellular DNA in the *Pseudomonas aeruginosa* biofilm matrix. Proc Natl Acad Sci
578 U S A 112:11353-8.
579 56. Irie Y, Roberts AEL, Kragh KN, Gordon VD, Hutchison J, Allen RJ, Melaugh G, Bjarnsholt T,
580 West SA, Diggle SP. 2017. The *Pseudomonas aeruginosa* PSL Polysaccharide Is a Social but
581 Noncheatable Trait in Biofilms. mBio 8.
582 57. Jennings LK, Dreifus JE, Reichhardt C, Storek KM, Secor PR, Wozniak DJ, Hisert KB, Parsek
583 MR. 2021. *Pseudomonas aeruginosa* aggregates in cystic fibrosis sputum produce exopolysaccharides
584 that likely impede current therapies. Cell Rep 34:108782.
585 58. Alhede M, Alhede M, Qvortrup K, Kragh KN, Jensen PO, Stewart PS, Bjarnsholt T. 2020. The
586 origin of extracellular DNA in bacterial biofilm infections in vivo. Pathog Dis 78.
587 59. Russo DM, Abdian PL, Posadas DM, Williams A, Vozza N, Giordano W, Kannenberg E,
588 Downie JA, Zorreguieta A. 2015. Lipopolysaccharide O-chain core region required for cellular cohesion
589 and compaction of *in vitro* and root biofilms developed by *Rhizobium leguminosarum*. Appl Environ
590 Microbiol 81:1013-23.
591 60. Mulcahy H, Sibley CD, Surette MG, Lewenza S. 2011. *Drosophila melanogaster* as an animal
592 model for the study of *Pseudomonas aeruginosa* biofilm infections *in vivo*. PLoS Pathog 7:e1002299.
593 61. Bjarnsholt T, Jensen PO, Fiandaca MJ, Pedersen J, Hansen CR, Andersen CB, Pressler T,
594 Givskov M, Hoiby N. 2009. *Pseudomonas aeruginosa* biofilms in the respiratory tract of cystic fibrosis
595 patients. Pediatr Pulmonol 44:547-58.
596 62. Heeb S, Itoh Y, Nishijyo T, Schnider U, Keel C, Wade J, Walsh U, O'Gara F, Haas D. 2000.
597 Small, stable shuttle vectors based on the minimal pVS1 replicon for use in gram-negative, plant-
598 associated bacteria. Mol Plant Microbe Interact 13:232-7.
599 63. Smith AW, Iglewski BH. 1989. Transformation of *Pseudomonas aeruginosa* by electroporation.
600 Nucleic Acids Res 17:10509.
601 64. Mayer-Hamblett N, Rosenfeld M, Gibson RL, Ramsey BW, Kulasekara HD, Retsch-Bogart GZ,
602 Morgan W, Wolter DJ, Pope CE, Houston LS, Kulasekara BR, Khan U, Burns JL, Miller SI, Hoffman
603 LR. 2014. *Pseudomonas aeruginosa in vitro* phenotypes distinguish cystic fibrosis infection stages and
604 outcomes. Am J Respir Crit Care Med 190:289-97.
605 65. Barrick JE, Lenski RE. 2013. Genome dynamics during experimental evolution. Nat Rev Genet
606 14:827-39.
607 66. Deatherage DE, Traverse CC, Wolf LN, Barrick JE. 2014. Detecting rare structural variation in
608 evolving microbial populations from new sequence junctions using breseq. Front Genet 5:468.
609 67. Schindelin J, Arganda-Carreras I, Frise E, Kaynig V, Longair M, Pietzsch T, Preibisch S,
610 Rueden C, Saalfeld S, Schmid B, Tinevez JY, White DJ, Hartenstein V, Eliceiri K, Tomancak P,
611 Cardona A. 2012. Fiji: an open-source platform for biological-image analysis. Nat Methods 9:676-82.
612 68. Davis MR, Jr., Muszynski A, Lollett IV, Pritchett CL, Carlson RW, Goldberg JB. 2013.
613 Identification of the mutation responsible for the temperature-sensitive lipopolysaccharide O-antigen
614 defect in the *Pseudomonas aeruginosa* cystic fibrosis isolate 2192. J Bacteriol 195:1504-14.

Figure 1

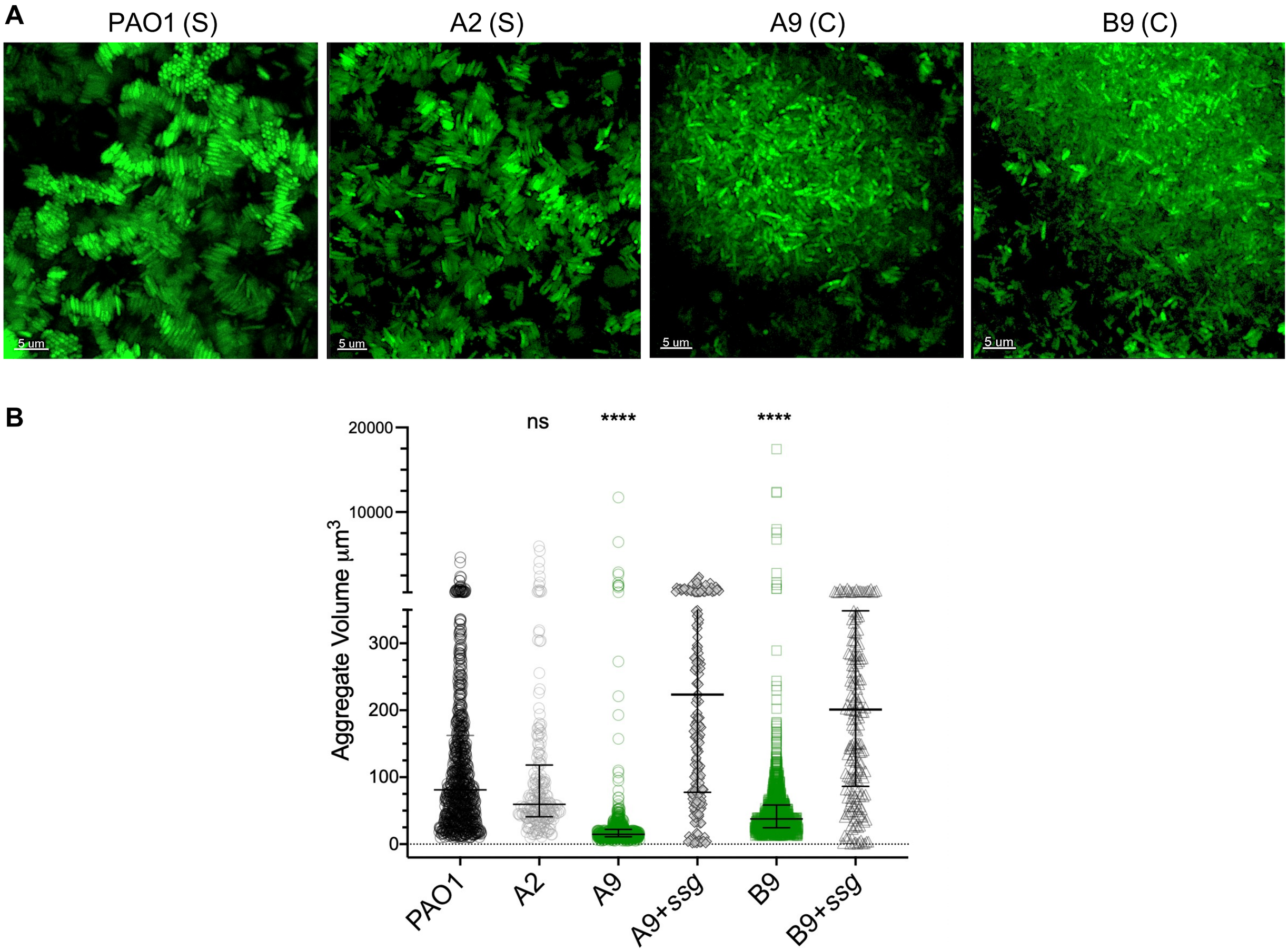
A
PAO1 (S)
A2 (S)
A9 (C)
B9 (C)
5 um
5 um
5 um
5 um
B
Aggregate Volume µm3
20000
10000
300
200
100
0
ns
****
****
PAO1
A2
A9
A9+ssg
B9
B9+ssg

Figure 2

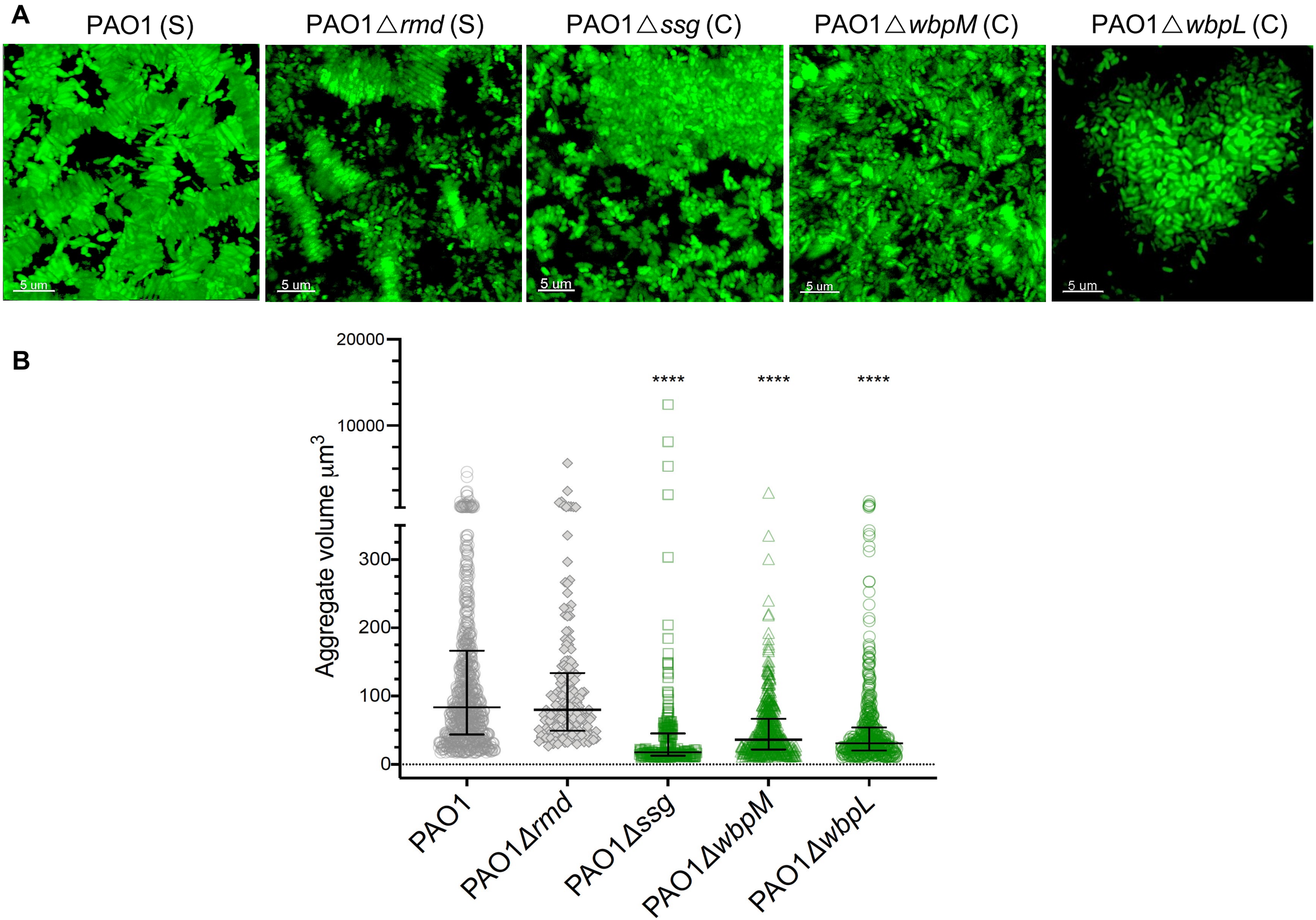
A
PAO1 (S)
PAO1△rmd (S)
PAO1△ssg (C)
PAO1△wbpM (C)
PAO1△wbpL (C)
5 um
B
Aggregate volume µm3
20000
10000
300
200
100
0
****
****
****
PAO1
PAO1Δrmd
PAO1Δssg
PAO1ΔwbpM
PAO1ΔwbpL

Figure 3

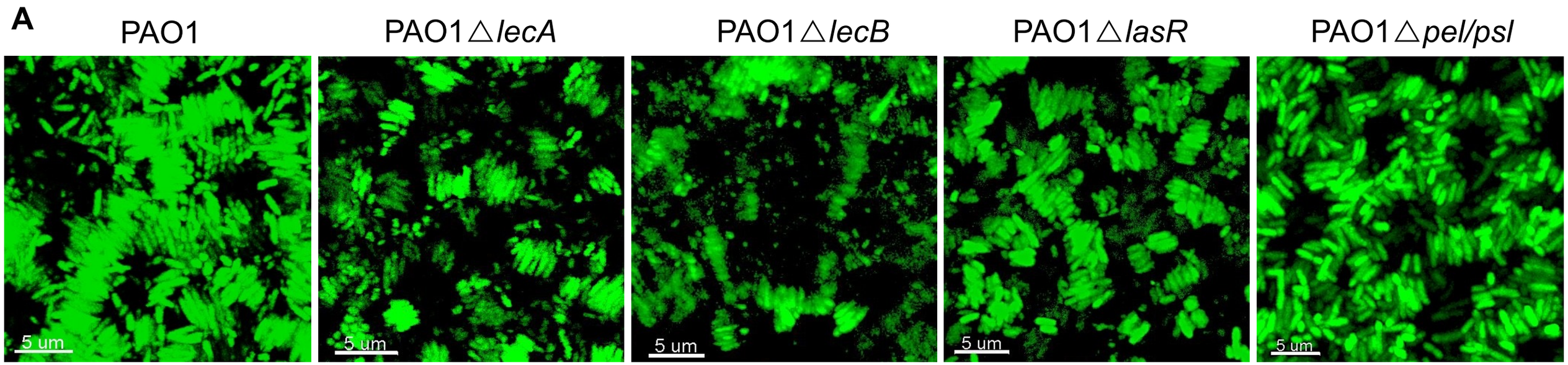
A
PAO1
PAO1△lecA
PAO1△lecB
PAO1△lasR
PAO1△pel/psl
5 um
5 um
5 um
5 um
5 um

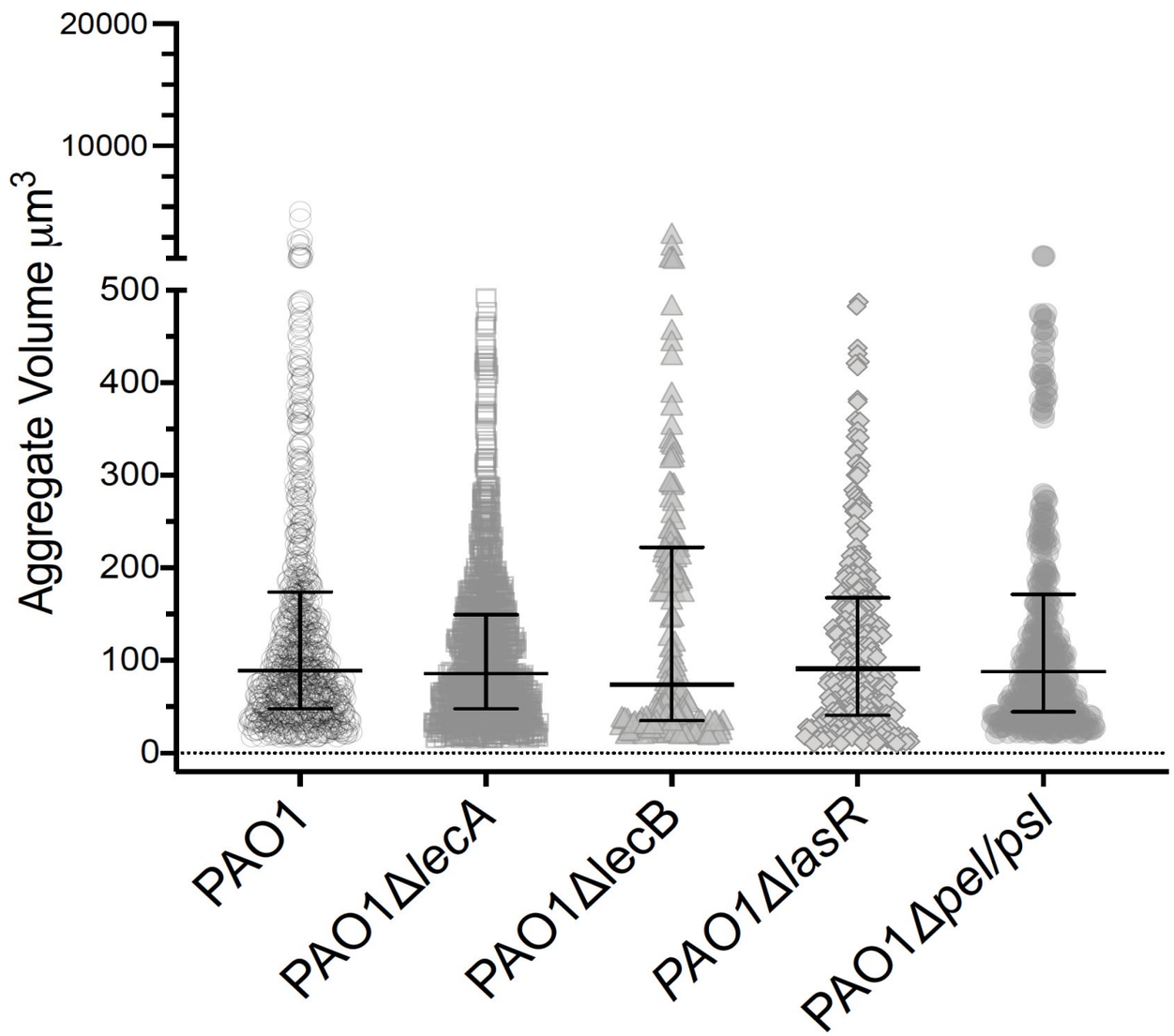
B
Aggregate Volume µm3
20000
10000
500
400
300
200
100
0
PAO1
PAO1ΔlecA
PAO1ΔlecB
PAO1ΔlasR
PAO1Δpel/psl

Figure 4

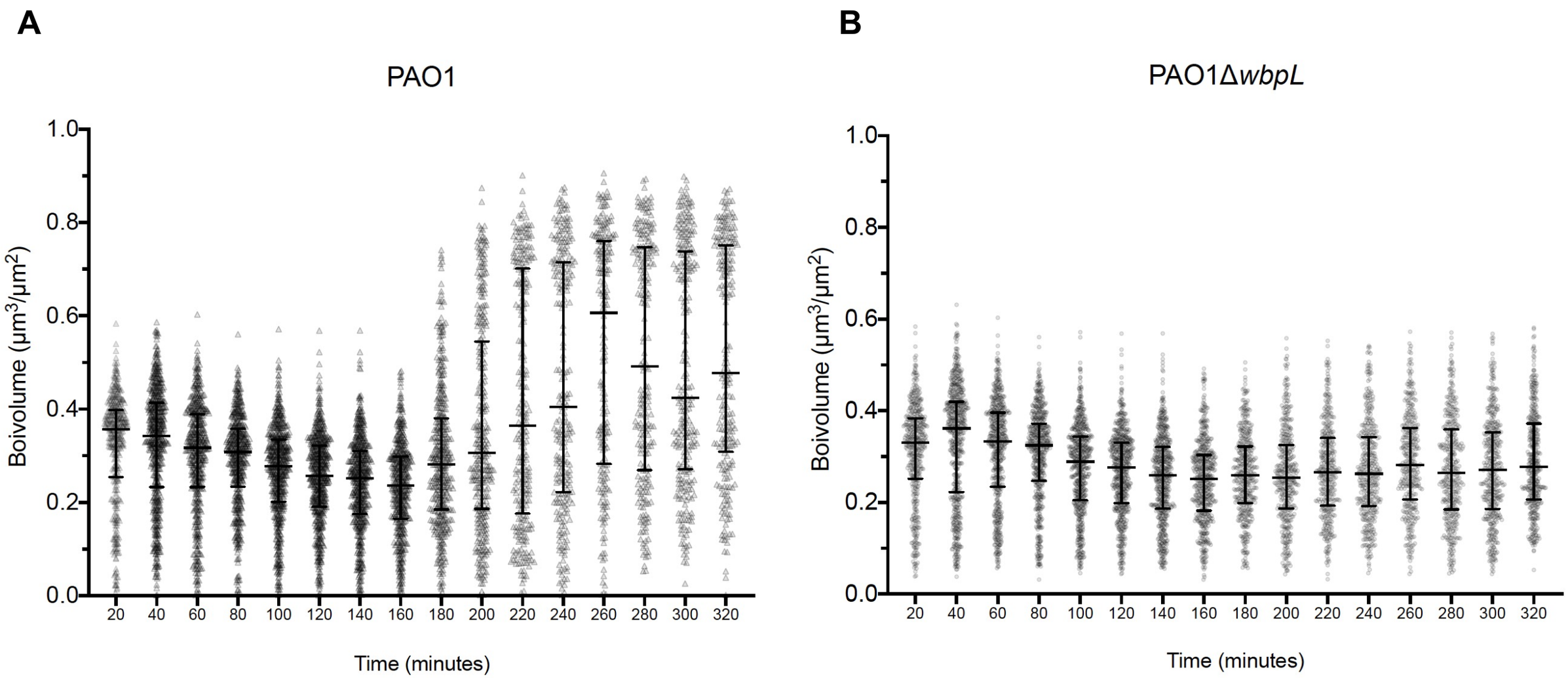
A
PAO1
Boivolume (µm3/µm2)
1.0
0.8
0.6
0.4
0.2
0.0
20 40 60 80 100 120 140 160 180 200 220 240 260 280 300 320
Time (minutes)
B
PAO1ΔwbpL
Boivolume (µm3/µm2)
1.0
0.8
0.6
0.4
0.2
0.0
20 40 60 80 100 120 140 160 180 200 220 240 260 280 300 320
Time (minutes)

Figure 5

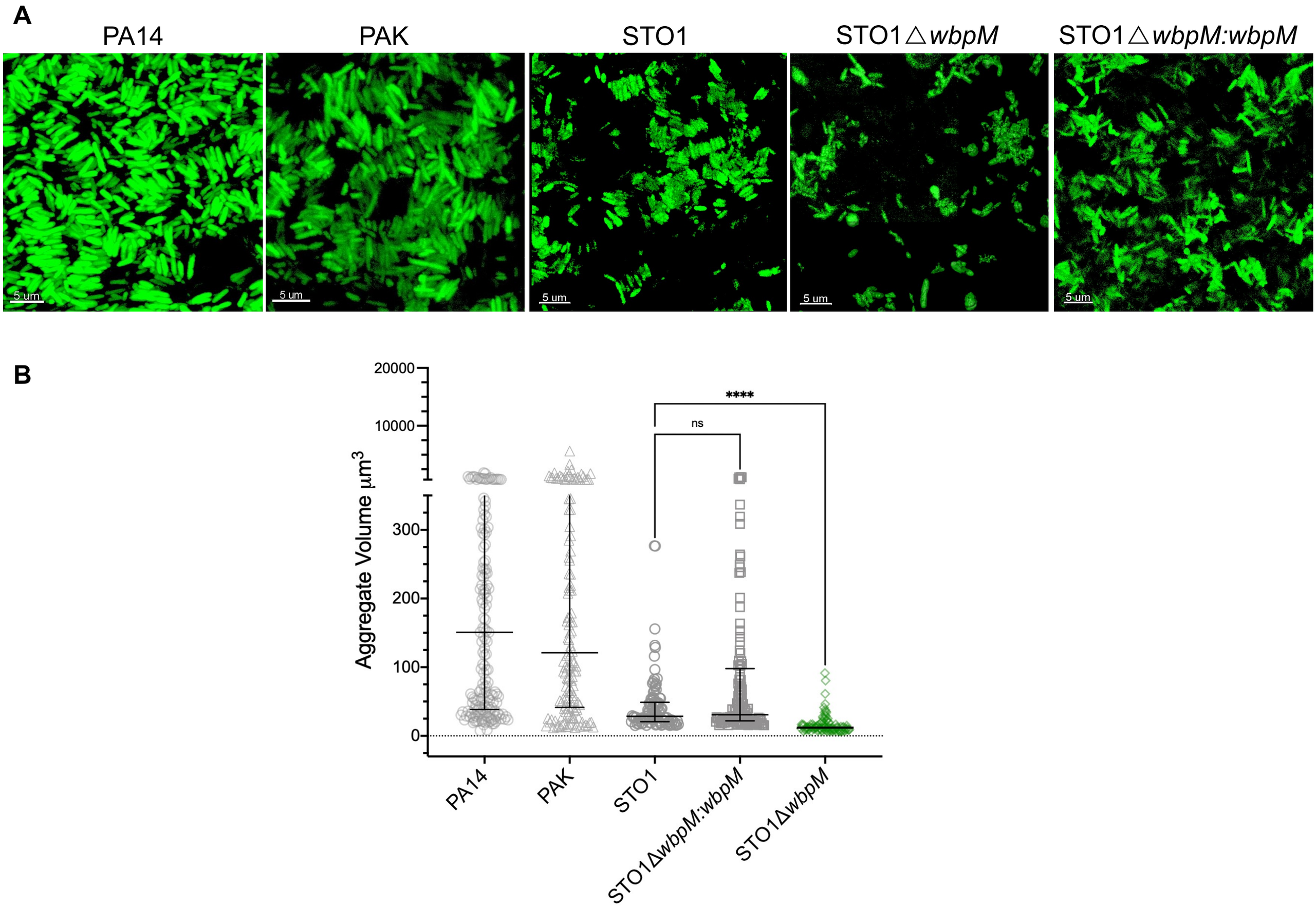
A
PA14
PAK
STO1
STO1△wbpM
STO1△wbpM:wbpM
5 um
B
Aggregate Volume µm3
20000
10000
300
200
100
0
****
ns
PA14
PAK
STO1
STO1ΔwbpM:wbpM
STO1ΔwbpM

Figure 6

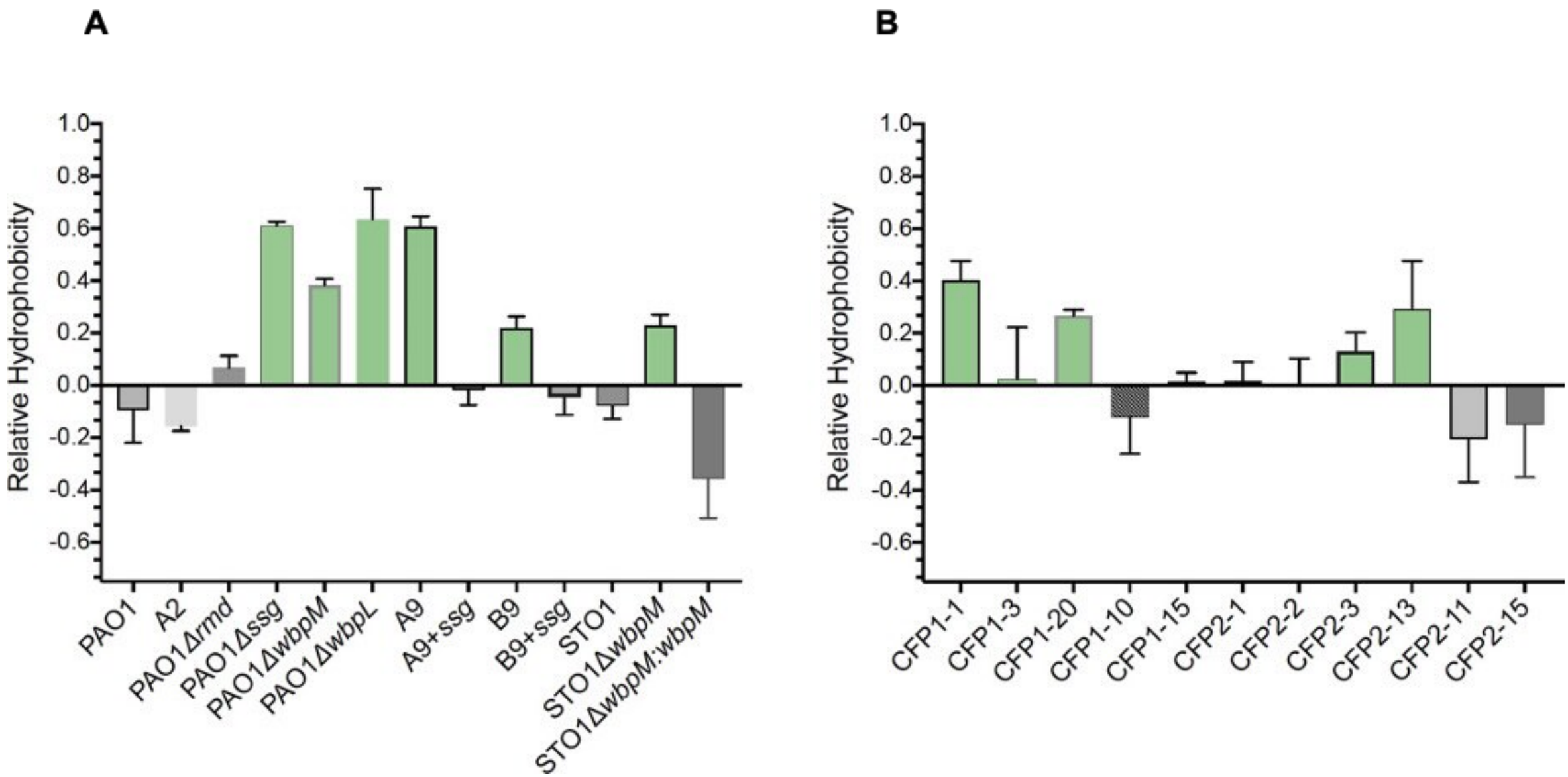
A
B
Relative Hydrophobicity
1.0
0.8
0.6
0.4
0.2
0.0
-0.2
-0.4
-0.6
PAO1
A2
PAO1Δrmd
PAO1Δssg
PAO1ΔwbpM
PAO1ΔwbpL
A9
A9+ssg
B9
B9+ssg
STO1
STO1ΔwbpM
STO1ΔwbpM:wbpM
CFP1-1
CFP1-3
CFP1-20
CFP1-10
CFP1-15
CFP2-1
CFP2-2
CFP2-3
CFP2-13
CFP2-11
CFP2-15

Figure S1

A

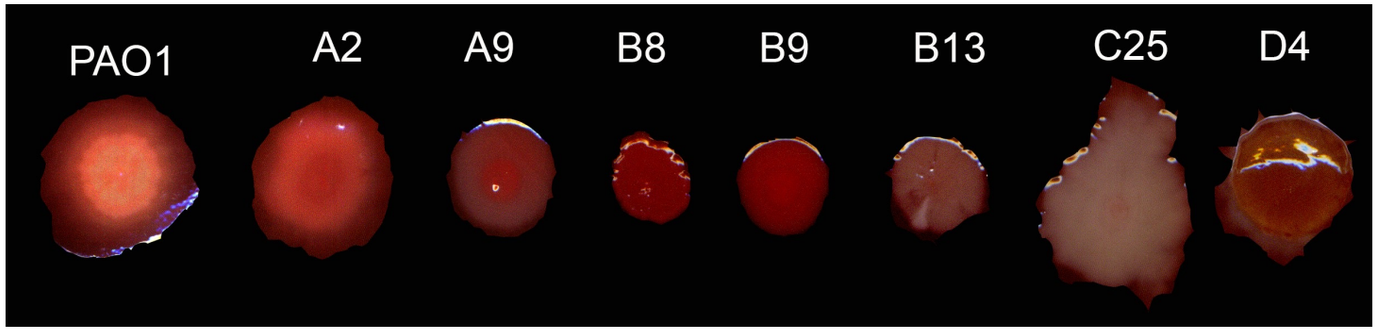

B

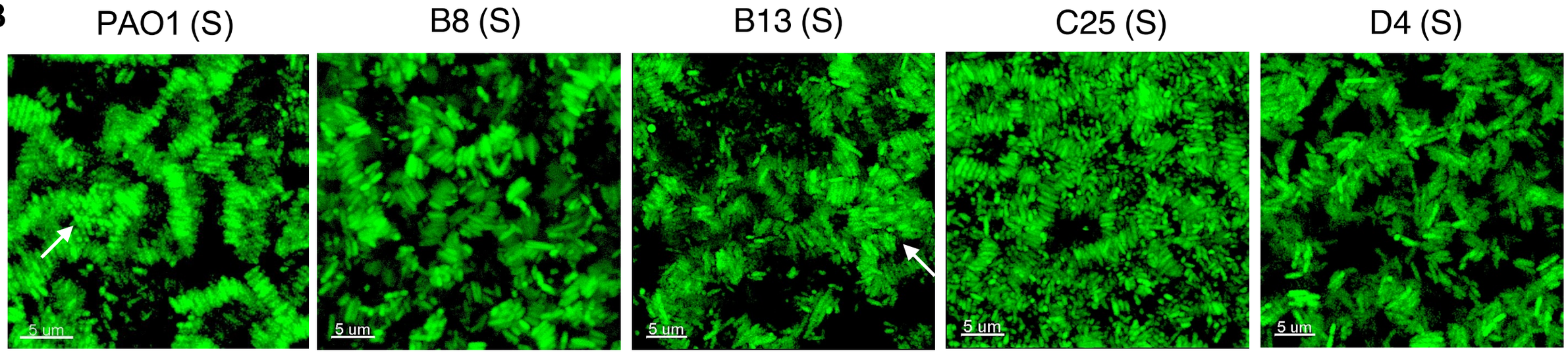

C

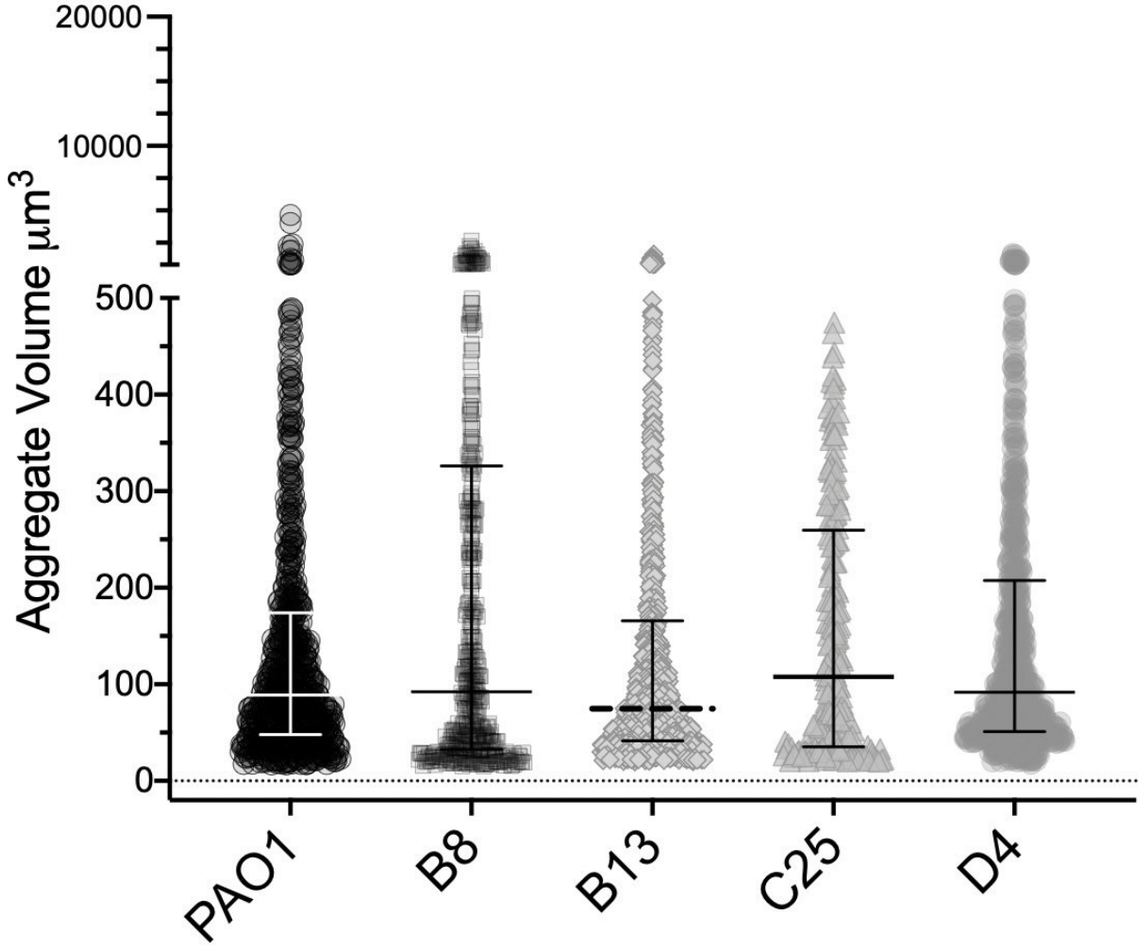

Figure S2

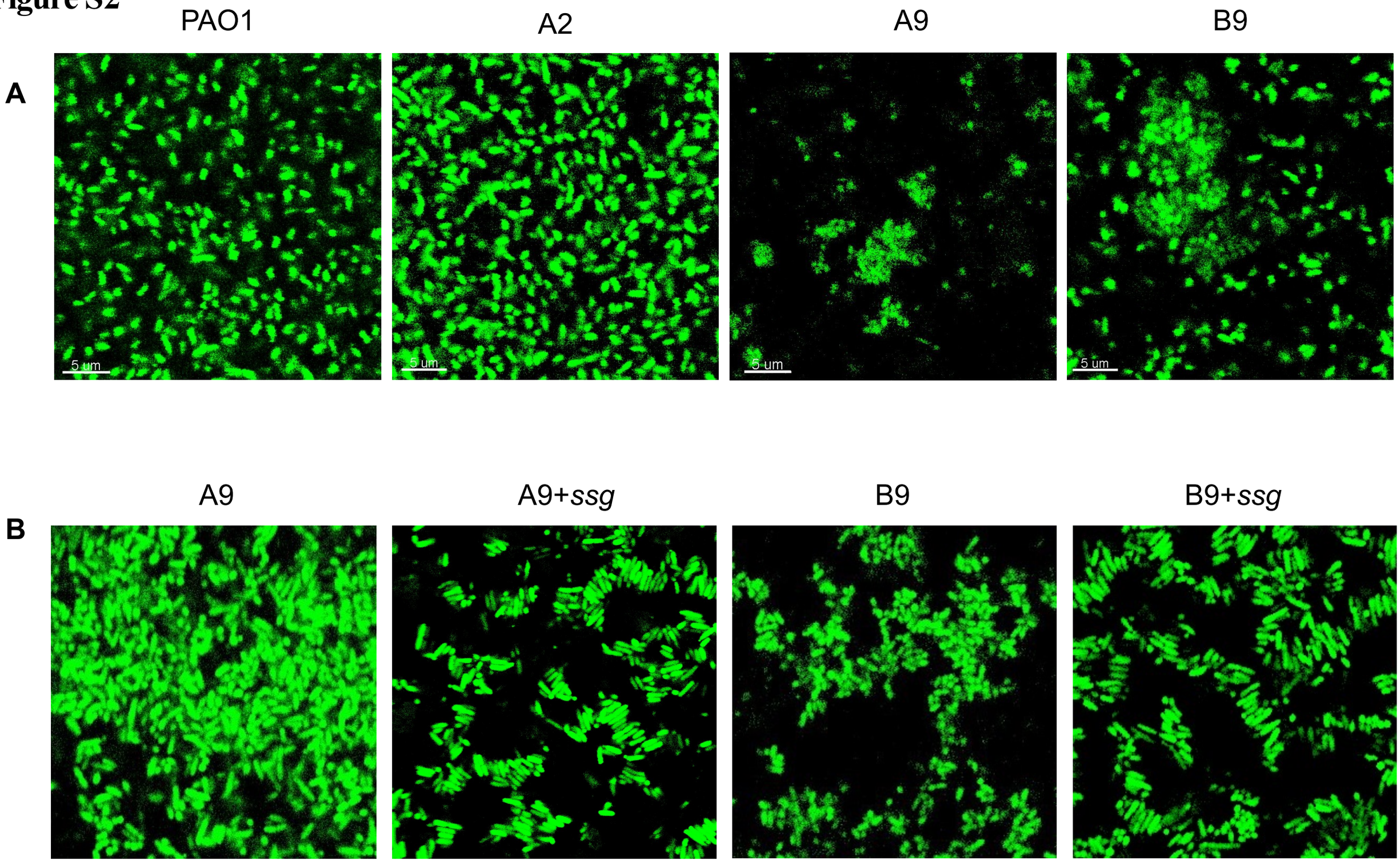

Figure S3

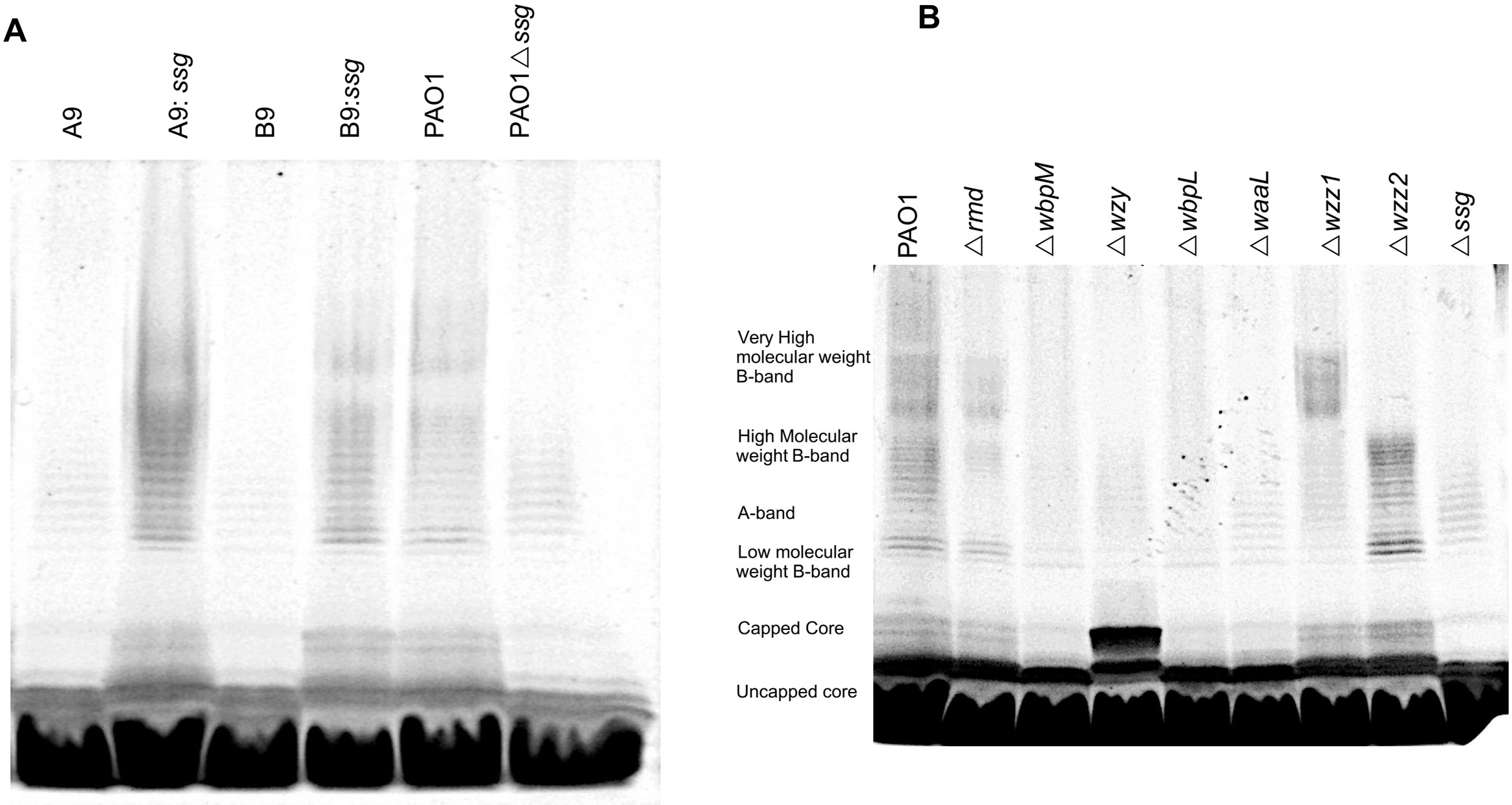
A
A9
A9: ssg
B9
B9:ssg
PAO1
PAO1△ssg
B
PAO1
△rmd
△wbpM
△wzy
△wbpL
△waaL
△wzz1
△wzz2
△ssg
Very High molecular weight B-band
High Molecular weight B-band
A-band
Low molecular weight B-band
Capped Core
Uncapped core

Figure S4

A

PAO1 (0.6 mg/ml DNA)
(5 mg/ml mucin)

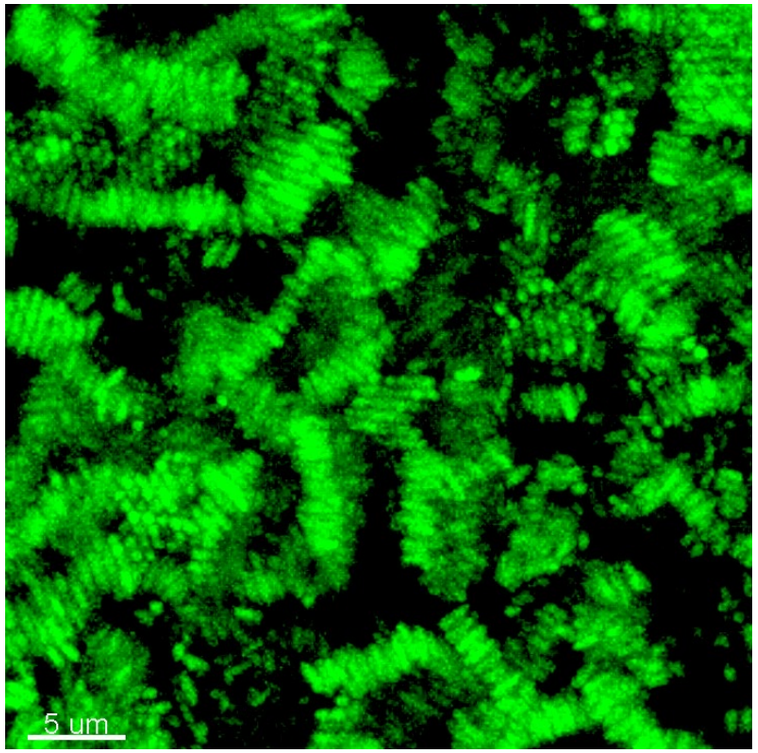

PAO1 (0.12 mg/ml DNA)
(1 mg/ml mucin)

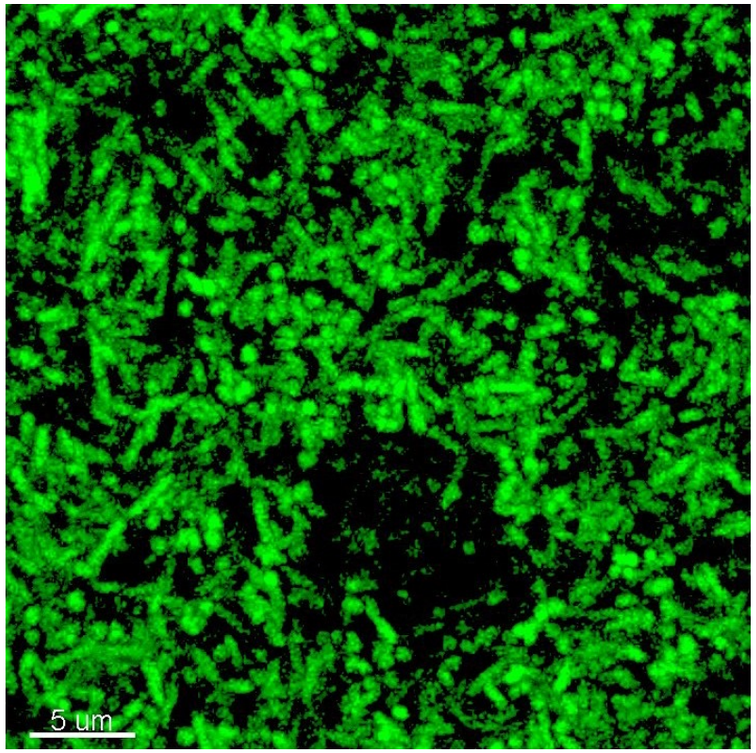

PAO1 (0.06 mg/ml DNA)
(0.5 mg/ml mucin)

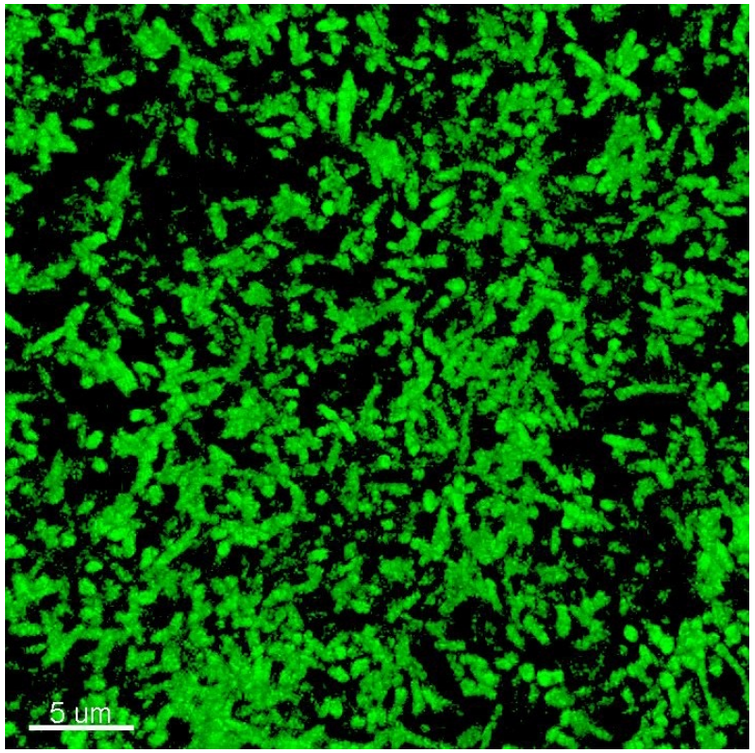

B

PAO1△*wbpL* (0.6 mg/ml DNA)
(5 mg/ml mucin)

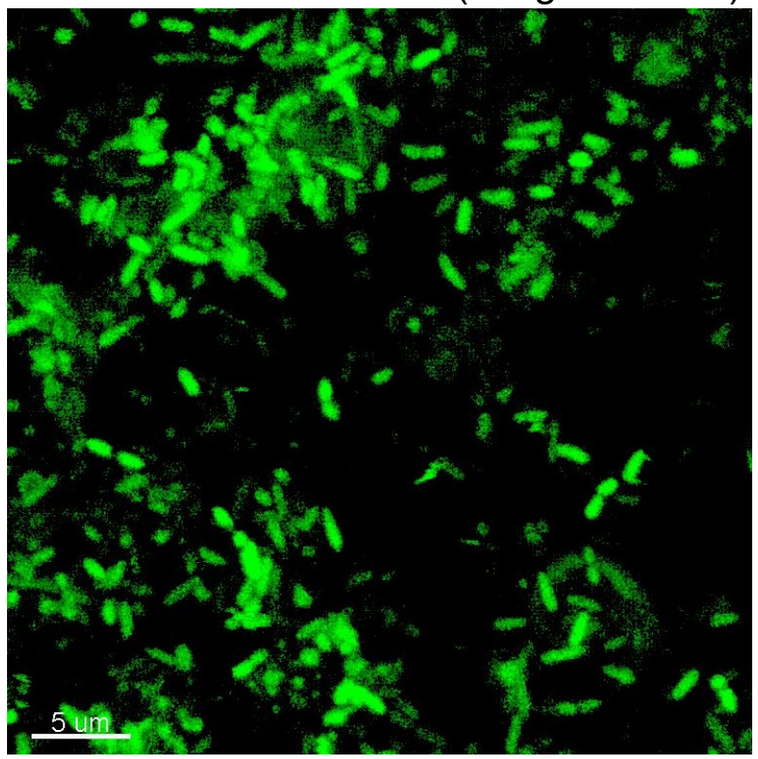

PAO1△*wbpL* (0.12 mg/ml DNA)
(1 mg/ml mucin)

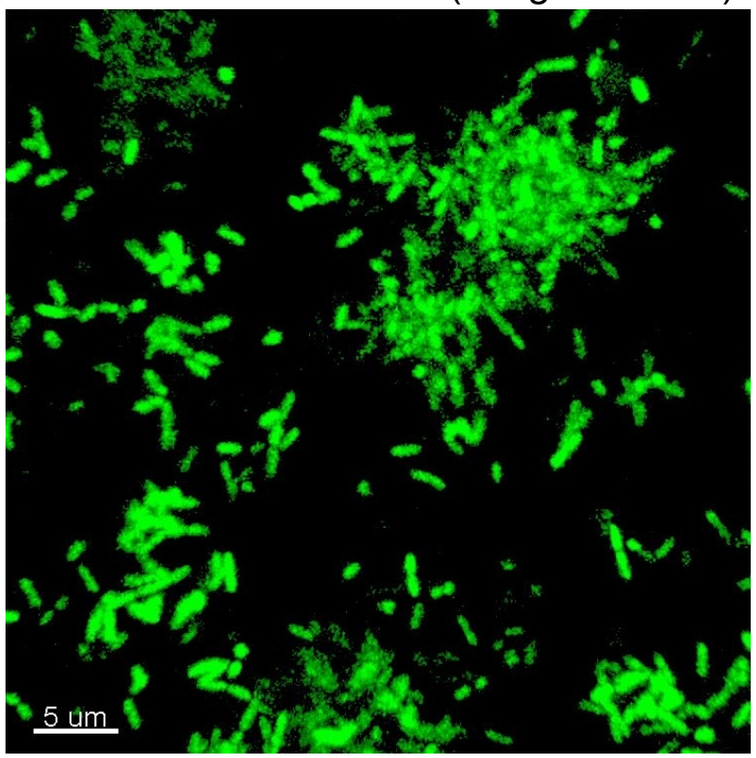

PAO1△*wbpL* (0.06 mg/ml DNA)
(0.5 mg/ml mucin)

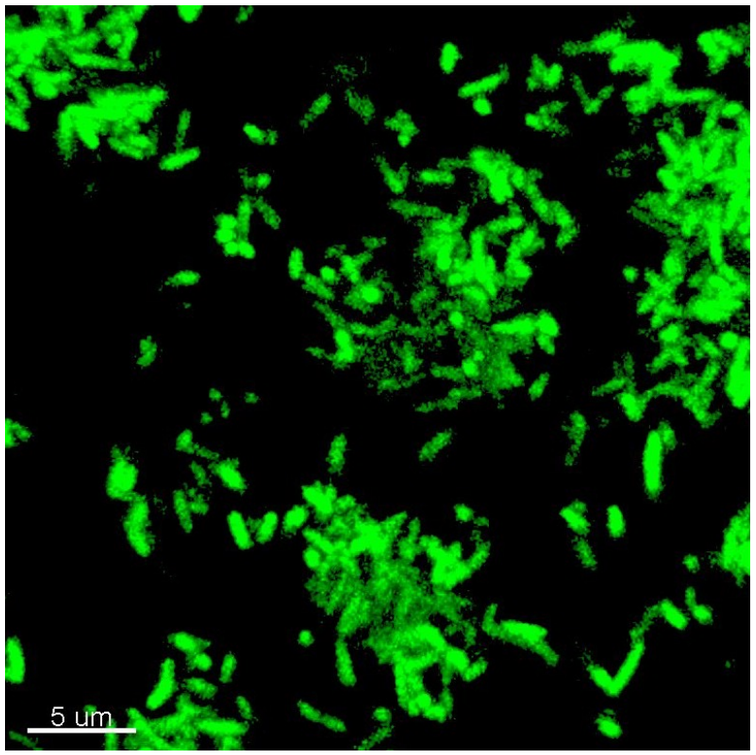

	PAO1	A2	A9	B9
Minimum	0.110031	0.12282713	0.100064	0.10049691
25% Percentile	0.248399	0.267627	0.222612	0.15592075
Median	0.35255	0.312206	0.277916	0.2315546
75% Percentile	0.41007625	0.393158	0.33127	0.33155867
Maximum	0.559253	0.600513	0.371328	0.469442558

***P. aeruginosa* strain**	**Description**		**Source**
PAO1	Wild type PAO1 (Nottingham strain)		Holloway collection
A2	Evolved PAO1 isolate	Evolved isolate	This study
A9	Evolved PAO1 isolate	Evolved isolate	This study
A9:*ssg*	Evolved PAO1 isolate complemented with *ssg* gene	Evolved isolate	This study
B8	Evolved PAO1 isolate	Evolved isolate	(1)
B9	Evolved PAO1 isolate	Evolved isolate	This study
B9:*ssg*	Evolved PAO1 isolate complemented with *ssg* gene	Evolved isolate	This study
B13	Evolved PAO1 isolate	Evolved isolate	This study
C25	Evolved PAO1 isolate	Evolved isolate	This study
D4	Evolved PAO1 isolate	Evolved isolate	This study
PAO1Δ*ssg*	PAO1 with *ssg* deletion	Isogenic mutant	This study
PAO1Δ*rmd*	PAO1 with *rmd* deletion/CPA^-		This study
PAO1Δ*wbpM*	PAO1 with *wbpM* deletion/OSA^-		This study
PAO1Δ*wbpL*	PAO1 with *wbpL* deletion/ CPA^- OSA^-		This study
PAO1Δ*waal*	PAO1 with *waal* deletion/ OSA^-		This study
PAO1Δ*wzy*	PAO1 with *wzy* deletion/ OSA^-		This study
PAO1Δ*wzz1*	PAO1 with *wzz1* deletion/No high molecular weight B-band		This study
PAO1Δ*wzz2*	PAO1 with *wzz2* deletion/No very high molecular weight B-band		This study
STO1	Clinical isolate of *P. aeruginosa* serotype O-1		[2]
PA14	PA14 wildtype		
PAK	PAK wildtype		
STO1Δ*wbpM*	Clinical isolate of *P. aeruginosa* serotype O-1/ OSA^-		[2]
STO1Δ*wbpM:wbpM*	Clinical isolate of *P. aeruginosa* serotype O-1; OSA^- / complemented with serotype O-1 *wbpM*		[2]
PAO1Δ*lecA*	PAO1 with *lecA* deletion		[3]
PAO1Δ*lecB*	PAO1 with *lecB* deletion		This study
PAO1Δ*pel/psl*	PAO1 with *pel/psl* deletions		[4]

PAO1Δ*lasR*	PAO1 with *lasR* deletion		This study
CFP1-1	CF isolate of *P. aeruginosa, isolated from* CFP1 sputum sample	Clinical isolate	This study
CFP1-3	CF isolate of *P. aeruginosa, isolated from* CFP1 sputum sample	Clinical isolate	This study
CFP1-10	CF isolate of *P. aeruginosa, isolated from* CFP1 sputum sample	Clinical isolate	This study
CFP1-15	CF isolate of *P. aeruginosa, isolated from* CFP1 sputum sample	Clinical isolate	This study
CFP1-20	CF isolate of *P. aeruginosa, isolated from* CFP1 sputum sample	Clinical isolate	This study
CFP2-1	CF isolate of *P. aeruginosa, isolated from* CFP2 sputum sample	Clinical isolate	This study
CFP2-2	CF isolate of *P. aeruginosa, isolated from* CFP2 sputum sample	Clinical isolate	This study
CFP2-3	CF isolate of *P. aeruginosa, isolated from* CFP2 sputum sample	Clinical isolate	This study
CFP2-11	CF isolate of *P. aeruginosa, isolated from* CFP2 sputum sample	Clinical isolate	This study
CFP2-13	CF isolate of *P. aeruginosa, isolated from* CFP2 sputum sample	Clinical isolate	This study
CFP2-15	CF isolate of *P. aeruginosa, isolated from* CFP2 sputum sample	Clinical isolate	This study

1. Azimi, S., et al., *Allelic polymorphism shapes community function in evolving Pseudomonas aeruginosa populations.* ISME J, 2020.
2. Davis, M.R., Jr., et al., *Identification of the mutation responsible for the temperature-sensitive lipopolysaccharide O-antigen defect in the Pseudomonas aeruginosa cystic fibrosis isolate 2192.* J Bacteriol, 2013. **195**(7): p. 1504-14.
3. Diggle, S. P., et al., *The galactophilic lectin, LecA, contributes to biofilm development in Pseudomonas aeruginosa*. Environ Microbiol, 2006. **8**(6): p. 1095-1104.
4. Irie, Y., et al., *The Pseudomonas aeruginosa PSL Polysaccharide Is a Social but Noncheatable Trait in Biofilms.* mBio, 2017. **8**(3).